

1 Citrus psorosis virus movement protein contains an aspartic protease required for
2 autocleavage and the formation of tubule-like structures at plasmodesmata

3

4 Gabriel Robles Luna^{a#}, Eduardo José Peña^a María Belén Borniego^{a*}, Manfred Heinlein^b,
5 María Laura García^a

6

7 Running title: MP^{CPsV} forms tubule structures at PD upon autocleavage

8

9 ^aInstituto de Biotecnología y Biología Molecular (IBBM), Facultad de Ciencias Exactas,
10 CONICET UNLP, La Plata, Argentina

11 ^bUniversité de Strasbourg, CNRS, IBMP UPR 2357, F-67000 Strasbourg, France

12

13 *Current address, Instituto de Investigaciones Fisiológicas y Ecológicas Vinculadas a la
14 Agricultura (IFEVA), Facultad de Agronomía, CONICET UBA C1417DSE, Buenos Aires,
15 Argentina

16

17 #Address correspondence to Gabriel Robles Luna, garobles@gmail.com

18

19 Word count abstract: 252

20 Word count text: 7688

21

22 **Abstract**

23 Plant virus cell-to-cell movement is an essential step in viral infections. This process is
24 facilitated by specific virus-encoded movement proteins (MPs), which manipulate the cell
25 wall channels between neighboring cells known as plasmodesmata (PD). Citrus psorosis
26 virus (CPsV) infection in sweet orange involves the formation of tubule-like structures
27 within PD, suggesting that CPsV belongs to “tubule-forming” viruses that encode MPs able
28 to assemble a hollow tubule extending between cells to allow virus movement. Consistent
29 with this hypothesis, we show that the MP of CPsV (MP^{CPsV}) indeed forms tubule-like
30 structures at PD upon transient expression in *Nicotiana benthamiana* leaves. Tubule
31 formation by MP^{CPsV} depends on its cleavage capacity, mediated by a specific aspartic
32 protease motif present in its primary sequence. A single aminoacid mutation in this motif
33 abolishes MP^{CPsV} cleavage, alters the subcellular localization of the protein and negatively
34 affects its activity in facilitating virus movement. The amino terminal 34 kDa cleavage
35 product (34K^{CPsV}), but not the 20 kDa fragment (20K^{CPsV}), supports virus movement.
36 Moreover, similar to tubule-forming MPs of other viruses, the MP^{CPsV} (and also the
37 34K^{CPsV} cleavage product) can homo-oligomerize, interact with PD-located Protein 1
38 (PDLP1) and assemble tubule-like structures at PD by a mechanism dependent on the
39 secretory pathway. 20K^{CPsV} retains the protease activity and is able to cleave a cleavage-
40 deficient MP^{CPsV} *in trans*. Altogether, these results demonstrate that CPsV movement
41 depends on the autolytic cleavage of MP^{CPsV} by an aspartic protease activity, which
42 removes the 20K^{CPsV} protease and thereby releases the 34K^{CPsV} protein for PDLP1-
43 dependent tubule formation at PD.

44

45 **Importance**

46 Infection by citrus psorosis virus (CPsV) involves a self-cleaving aspartic protease activity
47 within the viral movement protein (MP), which results in the production of two peptides
48 termed 34K^{CPsV} and 20K^{CPsV} that carry the MP and viral protease activities, respectively.
49 The underlying protease motif within the MP is also found in the MPs of other members of
50 the *Aspiviridae* family suggesting that protease-mediated protein processing represents a
51 conserved mechanism of protein expression in this virus family. The results also
52 demonstrate that CPsV and potentially other ophioviruses move by a tubule-guided

53 mechanism. Although several viruses from different genera were shown to use this
54 mechanism for cell-to-cell movement, our results also demonstrate that this mechanism is
55 controlled by post-translational protein cleavage. Moreover, given that tubule formation
56 and virus movement could be inhibited by a mutation in the protease motif, targeting the
57 protease activity for inactivation could represent an important approach for ophiovirus
58 control.
59

60 **Introduction**

61 The cell-to-cell spread of virus infection generally depends on the activity of one or more
62 virus-encoded movement proteins (MPs), which target intercellular communication
63 channels within the plant cell walls known as plasmodesmata (PD) (1, 2). These channels
64 provide both membrane and cytoplasmic continuity between cells and thus function as
65 intercellular conduits for both soluble and membrane-associated compounds, ranging from
66 small molecules such as salts, hormones and metabolites, to macromolecules, such as
67 proteins, short and long RNAs and protein:RNA complexes (3). Structurally, PD represent
68 unique structures, in which the plasma membrane (PM) and the endoplasmic reticulum
69 (ER) form two concentric membrane tubules extending through the cell wall and are in
70 close opposition to each other (ca. 10 nm) (4). The ER tubule (the ‘desmotubule’) is linked
71 from all its surface to the PM and, potentially, to the cell wall by proteinaceous spoke-like
72 extensions, which may represent specialized protein tethers that regulate the distance
73 between the two membranes and, thereby, the size of the cytoplasmic annulus available for
74 cytoplasmic transport (5). However, while this model for the regulation of the PD size
75 exclusion limit (SEL) remains speculative, numerous studies correlated the regulation of
76 PD function in controlling intercellular communication with the degree of callose
77 deposition in the cell wall surrounding the PD neck regions (6-8). Whereas the synthesis
78 and accumulation of callose in the cell wall causes the closure of the cytoplasmic
79 compartment by forcing the plasma membrane against the desmotubule, the degradation of
80 callose by beta-glucanases opens this compartment for intercellular transport (5).

81 Plant viruses exploit PD for their cell-to-cell movement by co-opting the cellular machinery
82 of PD-mediated transport. The cell-to-cell movement strategies used by viruses have been
83 deeply reviewed (9, 10) and classified into two general mechanisms based on the type of
84 alteration of PD structure. Whereas the tubule-guided mechanism involves the
85 displacement of the desmotubule by the formation of a tubule-like transport structure
86 assembled by multimerization of viral MP and the transport whole virions through the
87 tubule (9, 11-16), the non-tubule-guided mechanism usually occurs in the absence of virions
88 and does not involve structural alterations within PD but rather a viral interference with the
89 normal regulation of PD. Tobacco mosaic virus (TMV), the type virus using a non-tubule
90 guided mechanism, moves cell-to-cell independently of the coat protein (CP) (9, 17), by

91 targeting viral replication complexes (VRCs) to PD with the help of myosin motor
92 proteins(18). Moreover, this virus interferes with callose depositions at PD, thus allowing
93 the passage of the VRCs into the adjacent cell (19). The MP of this virus interacts with the
94 ER, microtubules and microtubule-associated proteins proposed to play a role in the
95 formation of movement-competent VRCs (20-22). There is evidence that the viral
96 movement process also involves the severing of actin filaments (23) and interactions of the
97 MP with synaptotagmin A (SYTA), which is proposed to act in endosomal recycling (24)
98 as well as a membrane tethering protein (5, 10, 25, 26).

99 Unlike the MP of TMV and presumably the MPs of other viruses moving by the non-
100 tubule-mediated mechanism, the MPs of tubule-forming viruses interact with members of
101 the PD-Located Protein (PDLP) family and this interaction is required for tubule assembly
102 and the spread of infection (27, 28). PDLPs require the ER-Golgi pathway for their
103 targeting to PD (27, 29), which may explain the observed sensitivity of tubule-formation
104 and tubule-mediated virus movement to secretory pathway inhibitors (27, 30, 31). DNA
105 and RNA viruses that move cell-to-cell by a tubule-guided mechanism have been found in
106 the *Caulimo-* (11, 27, 32, 33), *Seco-* (15, 27, 34-37), *Bunya-* (13, 38), and *Bromoviridae*
107 (39) families.

108 Citrus psorosis virus (CPsV), the type member of the *Aspiviridae* family (formerly
109 *Ophioviridae*), genus *Ophiovirus* (40, 41), is a three-partite, non-enveloped, negative-sense,
110 single-stranded (ss) RNA virus. RNA 1 encodes a 280 kDa replicase (42) as well as a 24
111 kDa protein that affects miRNA maturation (43) and has RNA silencing-suppressing
112 activity (44). RNA 2 encodes a protein of 54 kDa (named hereafter MP^{CPsV}), which
113 displays several features of a MP (45, 46) and has RNA silencing-suppressing activity as
114 well (44). RNA 3 encodes a CP of 48 kDa (47). In addition to CPsV, the *Ophiovirus* genus
115 contains six more members, Mirafiori lettuce big-vein virus (MiLBVV), blueberry mosaic
116 associated virus (BIMaV), lettuce ring necrosis virus (LRNV), freesia sneak virus (FSV),
117 ranunculus white mottle virus (RWMV) and tulip mild mottle mosaic virus (TMMMV), of
118 which the last two have not been completely sequenced and are less characterized.

119 Here we show that CPsV induces the formation of tubular structures at PD during infection
120 in citrus. Similar structures protruding from PD are observed by confocal laser scanning
121 microscopy (CLSM) upon ectopic expression of MP^{CPsV} fused to fluorescent markers. The

122 formation of the tubules is dependent on the proper localization of PDLP at PD. We also
123 show that the MP^{CPsV} is autocatalytically processed during both infection and transient
124 expression and that a conserved aspartic protease motif within MP^{CPsV} is responsible for
125 this activity. By further functional characterization, we demonstrate that the autocatalytic
126 cleavage releases an N-terminal peptide fundamental for tubule formation and a C-terminal
127 protein fragment with viral protease activity.

128

129 **Results**

130 **Cell walls of CPsV-infected citrus plants exhibit tubule-like structures**

131 To get insight into the cell-to-cell movement mechanism used by CPsV, we analyzed the
132 PD structure in CPsV-infected sweet orange plants. Ultrathin sections of healthy and
133 infected leaves harvested at similar developmental stages were sectioned and observed by
134 Transmission electron microscopy (TEM). In contrast to healthy samples (FIG. 1Ai) the PD
135 in the CPsV-infected sample contained a double line of electron-dense and well-organized
136 proteinaceous material, compatible with a longitudinal sectioning through a hollow tubular
137 structure that extended from the cell wall into the cytoplasm (FIG. 1Aii, arrow).

138 Given the capacity of ophiovirus MPs to target PD upon transient expression in *N.*
139 *benthamiana* leaves (46), we wanted to know whether these proteins form tubule-like
140 structures under these conditions. Expression of MP^{CPsV} N-terminally (FIG. 1Bi,
141 arrowhead) and C-terminally (FIG. 1Bii, arrows) fused to fluorescent proteins (*e.g.*
142 enhanced green fluorescent protein, GFP) revealed that MP^{CPsV} indeed can form tubules;
143 however, only the C-terminal fusion (MP^{CPsV}:GFP) showed tubule-like structures at PD
144 (FIG. 1Bii, arrows), whereas N-terminal fusions (GFP:MP^{CPsV}) labeled PD without forming
145 such structures. For cells expressing C-terminal fusion protein, the number of tubules per
146 cell was variable and each cell showed both tubular and non-tubular MP^{CPsV}:GFP at PD
147 (FIG. 1Bii). These observations indicate although both orientations target PD, only C-
148 terminal fusions to GFP can form tubular structures.

149

150 **The MP^{CPsV} interacts with PD-localized PDLP1 for tubule assembly**

151 Consistent with the tubule assembly from MP, the monomers of the tubule-forming MPs of
152 caulimo- and nepoviruses showed MP-MP interaction *in vivo* (27). Moreover, these

153 proteins were shown to interact with members of the PDLP family at PD (27, 28). Amari et
154 al. (27) showed that both the MP of grapevine fanleaf virus (GFLV) and the MP of
155 cauliflower mosaic virus (CaMV) interact with PDLPs at PDs, and that the systemic
156 movement of both viruses was inhibited in *pdlp1 pdlp2 pdlp3* triple knock-out *Arabidopsis*
157 *thaliana* mutants (27). The interaction with the PDLP family of proteins might be a
158 common feature of the tubule-forming viruses. Consistently, also the tubule-forming MP of
159 cowpea mosaic virus (CPMV) was shown to interact with PDLP1 *in vivo* (28). To
160 determine whether the MP^{CPsV} has the capacity to interact with PDLP1 we used
161 fluorescence lifetime imaging microscopy (FLIM) to measure the degree of fluorescence
162 resonance emission transfer (FRET) between the GFP and monomeric red fluorescent
163 protein (RFP) moieties of MP^{CPsV}:GFP and PDLP1:RFP expressed in *N. benthamiana*
164 epidermal cells. When MP^{CPsV}:GFP was expressed alone, the average fluorescence lifetime
165 (τ) of GFP was $2,1 \pm 0.1$ ns ($n = 65$) (FIG. 2Ai and v). A similar τ value of $2,1 \pm 0.08$ ns (n
166 $= 59$) was measured when this protein was co-expressed with PD callose-binding protein 1
167 fused to the red fluorescent protein Cherry (PDCB1:Cherry) (48) (FIG. 2Aii and v). When
168 MP^{CPsV}:GFP was co-expressed with an RFP-tagged version of the MP^{CPsV} (MP^{CPsV}:RFP),
169 the τ value was $1,9 \pm 0.1$ ns ($n = 30$). This value is significantly different ($P < 0,01$) from the
170 τ value observed when MP^{CPsV}:GFP was expressed alone and represents a FRET efficiency
171 of 10% (FIG. 2Aiii and v), thus indicating the capacity of MP^{CPsV} to oligomerize. Co-
172 expression of MP^{CPsV}:GFP with PDLP1:RFP resulted in a τ -value of $2,0 \pm 0.1$ ns ($n = 78$)
173 (5% FRET), which also differed significantly ($P < 0,01$) from the τ -value obtained when
174 MP^{CPsV}:GFP was expressed alone (FIG. 2Aiv and v). Given that the efficiency of FRET
175 depends on intermolecular vicinity between GFP and RFP moieties, we wondered whether
176 the FRET efficiency could be altered upon changing the position of the GFP fusion to
177 MP^{CPsV} from the C-terminus to the N-terminus. The average fluorescence lifetime (τ) of
178 GFP was $2,47 \pm 0.04$ ns ($n = 65$) when the GFP:MP^{CPsV} fusion protein was expressed alone
179 (FIG. 2Bi and v). A similar τ value was measured when this protein was co-expressed with
180 PD callose-binding protein 1 PDCB1:Cherry (48) (FIG. 2Bii and v). When GFP:MP^{CPsV}
181 was co-expressed with MP^{CPsV}:RFP, the τ value was $2,1 \pm 0.1$ ns ($n = 76$). This value is
182 significantly different ($P < 0,01$) from the τ value observed when GFP:MP^{CPsV} was
183 expressed alone and represents a FRET efficiency of 15% (FIG. 2Biii and v), thus showing

184 again MP-MP oligomerization irrespective of the orientation of the GFP fusion to the
185 protein. Co-expression of GFP:MP^{CPsV} with PDLP1:RFP resulted in a τ -value of 1.9 ± 0.1
186 ns (n = 42) (23% FRET), which also differed significantly ($P < 0.01$) from the τ -value
187 obtained when GFP:MP^{CPsV} was expressed alone (FIG. 2Biv and v). These results confirm
188 that the MP^{CPsV} has the capacity to oligomerize and to interact with PDLP1.

189 PDLPs are targeted to PD via the ER-Golgi secretory pathway (29) through COPII vesicles
190 which are formed at ER-exit sites (49). The vesicle formation is dependent on Sar1, a Ras-
191 like small GTPase. Consistently, the expression of a dominant-negative mutant of
192 Sar1[H74L], inhibited COPII vesicle formation and thus PDLP targeting to PD (49, 50). To
193 test if the inhibition of PDLP targeting to PD affects the tubule formation by MP^{CPsV} at PD,
194 we transiently expressed PDLP1:RFP or MP^{CPsV}:RFP together with either Sar1[H74L]:GFP
195 or with the wild type Sar1:GFP as control. Co-expression with the wild type Sar1:GFP
196 showed no effect on the targeting of PDLP1:RFP to PD (FIG. 2Ci and ii) and the ability of
197 MP^{CPsV} to assemble tubule-like structures at PD (FIG. 2Di, ii and Table 1). However, co-
198 expression with Sar1[H74L]:GFP inhibited PDLP1:RFP accumulation of at PD (FIG. 2Ciii
199 and iv) and as previously shown, it remains located at the ER (27, 29). In addition, although
200 the MP^{CPsV}:RFP was detected at PD, as seen by callose co-staining with aniline blue, the
201 ability of MP^{CPsV}:RFP to form tubule-like structures was inhibited (FIG. 2Diii, iv and Table
202 1). Thus, the ability of MP^{CPsV} to assemble tubules requires an intact ER-Golgi pathway.

203

204 **MP^{CPsV} GFP-fusion orientation and protein processing determines cell-to-cell** 205 **movement activity**

206 Given that MP^{CPsV}:GFP, but not GFP:MP^{CPsV}, is capable of forming tubules at PD, we
207 wondered whether this has functional relevance in virus movement. Since an infectious
208 cDNA clone of CPsV to test this hypothesis by a reverse genetic approach is not available,
209 we used an alternative assay to evaluate this activity (45, 46). In this assay we analyzed the
210 capacity of MP^{CPsV}:GFP and GFP:MP^{CPsV} to trans-complement TMV Δ MP Δ CP-GFP, a
211 previously reported movement-deficient TMV derivative (45). Highly diluted
212 Agrobacterium cultures harboring the TMV Δ MP Δ CP-GFP-encoding plasmid were
213 infiltrated together with cultures for the expression of either MP^{CPsV}:GFP, GFP:MP^{CPsV} or
214 GFP as a negative control. The sizes of the highly GFP-fluorescent infection foci grown by

215 viral cell-to-cell movement from initially TMV Δ MP Δ CP-GFP inoculated cells were
216 measured at 5 days post agroinfiltration (dpi). MP^{CPsV}:GFP- and GFP:MP^{CPsV}-expressing
217 tissues exhibited larger foci than the GFP-expressing control tissues, indicating that MP^{CPsV}
218 complements TMV Δ MP Δ CP-GFP cell-to-cell movement irrespective whether fused to
219 GFP at the N- or C-terminus (FIG.3A). Nevertheless, the infection foci complemented by
220 GFP:MP^{CPsV} were significantly smaller ($P < 0,01$) than those complemented by MP^{CPsV}:GFP
221 (FIG. 3A).

222 Immunoblot analysis using antibodies against the fused fluorescent protein tags showed
223 that both fusion proteins were expressed at a similar level (FIG. 3B), suggesting that the
224 difference in complementation efficiency between GFP:MP^{CPsV} and MP^{CPsV}:GFP is not
225 caused by a dose-dependent effect on movement activity. Surprisingly, expression of the C-
226 terminal fusion protein (MP^{CPsV}:GFP) led to the production of a 79 kDa protein and a
227 smaller GFP-containing protein of ≈ 48 kDa. Interestingly, expression of the N-terminal
228 fusion protein (GFP:MP^{CPsV}) led to production of a GFP containing protein of ≈ 69 kDa in
229 addition to the expected 82 kDa protein (FIG. 3B). *In silico* analysis with TargetP software
230 (51) showed that MP^{CPsV} encodes a N-terminal chloroplast transit peptide (cTP) (FIG 3.C).
231 Because these signals are cleaved upon chloroplast import, the 3 kDa mass difference
232 observed between MP^{CPsV}:GFP and GFP:MP^{CPsV}, could be a consequence of protein import
233 at the chloroplast. In agreement with this hypothesis, we found that only the C-terminal
234 fusion protein accumulates at chloroplasts (FIG. 3C).

235 Importantly, the expression profiles of the additional GFP-containing proteins are
236 compatible with a post-translational cleavage event, in which two MP^{CPsV} peptides of
237 34kDa and 20 kDa (N- and C-terminal fragments, respectively) are produced.

238

239 **The MP^{CPsV} contains a functional aspartic protease motif**

240 The occurrence of MP^{CPsV} protein fragments was also observed in protein extracts of
241 CPsV-infected *Chenopodium quinoa* plants using an antiserum against MP^{CPsV}. In these
242 extracts a band of approximately 54 kDa corresponding to full length MP^{CPsV}, and two
243 other bands of 34kDa and 20 kDa were seen (52). To further test these previous
244 observations, we repeated the immunoblot analysis using protein extracts from the systemic
245 host *Nicotiana occidentalis* P1 infected with CPsV. As shown in FIG. 4A, the MP^{CPsV}-

246 specific antibody indeed detected again the three distinct bands of 54 kDa, 34 kDa and 20
247 kDa, thus confirming the expression of three RNA 2-specific proteins during infection.

248 To address the origin of the observed MP^{CPsV} fragments, we analyzed the aminoacid
249 sequence of the protein using the HHpred software package (53). We identified a region
250 between aminoacids 331 and 413 of MP^{CPsV} showing aminoacid sequence similarity with
251 the catalytic aspartic site of cathepsin D as well as retroviral proteases, such as the protease
252 of HIV-2 (FIG. 4Bi). Consistently, also the MP of the ophiociruses MLBVV (MP^{MLBVV})
253 (protein id: AAN60448.1, region: 360-438) and BIMaV (MP^{BIMaV}) (protein id: AIF28243.1,
254 region: 368-450) showed sequence similarity with retroviral proteases and cathepsin D
255 (FIG. 4Bii and iii). The identified region in MP^{CPsV} contains an aspartic residue (D), which
256 is also the first aminoacid of an aminoacid triad that is strictly conserved among
257 ophiociruses MPs (45). This finding suggests that MP^{CPsV} and other ophiocirus MPs have
258 an autocatalytic protein cleavage activity.

259 To determine the location of the proteolytic cleavage site within the MP^{CPsV} aminoacid
260 sequence, we aligned the MP^{CPsV} sequence with HIV-1 protease substrate peptides (54). We
261 found that all these peptides aligned to the aminoacid sequence ₃₀₅NLSNFLADQR₃₁₄ of
262 MP^{CPsV} (FIG. 4B), which is compatible with the location of a cleavage site expected to
263 result in the formation of 34kDa and 20 kDa cleavage products. To identify the cleavage
264 site, we expressed MP^{CPsV}:GFP and GFP (negative control) in *N. benthamiana* and
265 immunopurified these proteins with anti-GFP agarose beads followed by on-bead tryptic
266 digestion and identification of the peptide by LC MS/MS. MS/MS spectra corresponding to
267 peptides with only one end compatible with trypsin digestion and found in three
268 independent MP^{CPsV}:GFP expressing samples and immunopurification experiments were
269 analyzed. MS/MS spectra indicate the existence of peptides derived from the C-terminal
270 end of the 34 kDa protein (FIG. 4 Ci) and another from the N-terminal end of the 20 kDa
271 protein (FIG. 4Cii) compatible with a cleavage between the aminoacids ₃₁₀LA₃₁₁.

272 To further prove that MP^{CPsV} contains an active aspartic protease motif responsible for the
273 observed cleavage products, we mutated the respective sequence motifs within MP^{CPsV} and
274 studied the effect of the mutations on the proteolytic processing of the protein. Site-directed
275 mutagenesis was used to replace the predicted catalytic Asp residue (D340) by Ala (A) or
276 Asn (N), and the mutant derivatives of MP^{CPsV} were named hereafter MP^{CPsV}D340A and

277 MP^{CPsV}D340N, respectively (FIG. 4D). Additionally, we constructed GFP and RFP fusions
278 to the 34K^{CPsV} (N-terminal cleavage product) and 20K^{CPsV} (C-terminal cleavage product)
279 proteins (FIG. 4D). The same approach was used to construct protein with mutations at the
280 cleavage site. Thus aminoacids at ₃₁₀LA₃₁₁ were replaced by an Asp residue, thereby
281 leading to two protein mutants named MP^{CPsV}L310D and MP^{CPsV}A311D. We also created
282 MP mutants named MP^{CPsV}A311R and MP^{CPsV}A311H in which the Ala at the position 311
283 was replaced by Arg or His respectively. Upon transient expression in *N. benthamiana*,
284 both MP^{CPsV}D340A and MP^{CPsV}D340N fused to RFP occurred with their expected sizes of
285 79 kDa (FIG. 4E). However, the 48 kDa cleavage product observed for MP^{CPsV}:RFP was
286 not detected for these mutants, which indicates that the aminoacid D340 is indeed critical
287 for protein cleavage (FIG. 4E). As expected, expression of the fluorescent protein-fused
288 20K^{CPsV} and 34K^{CPsV} proteins were detected as immuno-reactive bands of 48 kDa and 62
289 kDa, respectively (FIG. 4E). The four mutant proteins MP^{CPsV}L310D, MP^{CPsV}A311D,
290 MP^{CPsV}A311R and MP^{CPsV}A311H that carry mutations at the cleavage site showed a
291 cleavage product as observed for the MP^{CPsV} upon expression in C-terminal fusion to RFP.
292 Thus, none of the mutations introduced at the protein cleavage location prevented the
293 aspartic protease motif to recognize and cleave the protein at this location (FIG. 4E).

294

295 **MP^{CPsV} self-cleavage determines subcellular localization**

296 Next, we used confocal fluorescence microscopy to determine whether the introduced
297 mutations in the sites involved in catalytic cleavage of MP^{CPsV} affect the subcellular
298 localization of the protein. MP^{CPsV}:GFP localized to PD, tubule-like structures at PD,
299 nucleus, chloroplast (FIG. 3C), cytoplasm and microtubules, as previously described (52)
300 (FIG. 5A). In comparison, expression of MP^{CPsV}D340A:GFP led to a strongly reduced
301 nuclear localization of the GFP signal suggesting that the nucleus may accumulate the MP
302 cleavage products rather than the full-length protein. Instead, GFP signal was more strongly
303 associated with chloroplasts. Importantly, MP^{CPsV}D340A:GFP accumulated at PD but
304 failed to form tubule-like structures (FIG. 5B). The same subcellular localization pattern
305 was also obtained for MP^{CPsV}D340N:GFP (FIG. 5C). Expression of 34K^{CPsV}:GFP led to the
306 localization of GFP fluorescence exclusively at chloroplasts and also at PD, where it
307 formed tubular-like structures (FIG. 5D). In contrast, expression of 20K^{CPsV}:GFP led to

308 diffuse GFP fluorescence in the cytoplasm and nucleus (FIG. 5E) and showed no other
309 specific subcellular localization. The presence of tubule-like structures at PD in cells
310 expressing either MP^{CPsV}:GFP or 34K^{CPsV}:GFP, and the absence of the tubule-like
311 structures in cells expressing MP^{CPsV}D340A:GFP or MP^{CPsV}D340N:GFP indicates that the
312 cleavage of MP^{CPsV} by the aspartic protease motif is a prerequisite for tubule formation.
313 Since the full-length MP^{CPsV} is not able to form tubules, the fluorescent tubules observed in
314 MP^{CPsV}:GFP samples are likely formed by the unfused 34K^{CPsV} cleavage product, which
315 allow the incorporation of the full-length MP^{CPsV}:GFP protein into these structures.

316

317 **The 20K^{CPsV} cleavage product is an aspartic viral protease**

318 Since the protein cleavage mechanism used by aspartic proteases involves two catalytic
319 triads (55), the 20K^{CPsV} cleavage product that retains the aspartic protease activity should
320 also retain a capacity to dimerize. To test this hypothesis, we measured the fluorescence
321 lifetime of 20K^{CPsV}:GFP upon co-expression with 20K^{CPsV}:RFP. Under these conditions,
322 the τ of 20K^{CPsV}:GFP localized at the nucleus was $2,37 \pm 0.05$ ns ($n = 23$) and a very similar
323 fluorescence lifetime of 20K^{CPsV}:GFP of $2,32 \pm 0.05$ ns ($n = 14$) was measured when
324 expressed together with RFP as a negative control ($P < 0,01$). A significantly lower τ value
325 was determined when 20K^{CPsV}:GFP was co-expressed with 20K^{CPsV}:RFP ($2,16 \pm 0.08$ ns; n
326 = 19; $P < 0,01$), representing a FRET efficiency of 9 %. Similar fluorescence lifetime
327 measurements were repeated by focusing on the proteins localized in the cytoplasm. Here,
328 the 20K^{CPsV}:GFP and 20K^{CPsV}:RFP underwent FRET with an efficiency of 14% (FIG. 6A
329 iii and v). These observations indicate that the cleaved 20K^{CPsV} peptide retains the ability to
330 dimerize and thereby to form the dimeric catalytic triad proposed to be involved in its
331 protease activity.

332 Next, we wondered whether the aspartic protease activity of MP^{CPsV} can recognize and
333 process its target *in trans*. Immunoblot analysis of extracts derived from agro-infiltrated *N.*
334 *benthamiana* leaves co-expressing MP^{CPsV}:RFP together with the proteolytic activity-
335 deficient mutant MP^{CPsV}D340A:GFP revealed that full length protein, and/or the
336 20K^{CPsV}:RFP autocleavage product efficiently cleaves the MP^{CPsV}D340A:GFP *in trans*
337 (FIG. 6B; immunoblots on the left). The trans-acting proteolytic activity indeed resides in
338 the cleaved 20K^{CPsV} peptide, as was confirmed upon coexpression of MP^{CPsV}D340A:GFP

339 with 20K^{CPsV}:RFP (FIG. 6B; immunoblots on the right). Consistent with
340 MP^{CPsV}D340A:GFP cleavage by MP^{CPsV}:RFP or 20K^{CPsV}:RFP, green fluorescent tubule-
341 like structures were seen at PD (FIG. 6C). Thus, MP^{CPsV} has the capacity to execute
342 cleavage *in trans* as well as *in cis* and the protease activity segregates with the aspartic
343 protease within the cleaved 20K^{CPsV} protein fragment upon cleavage.

344

345 **Cell-to-cell movement activity depends on the 34K protein**

346 The effect of the MP^{CPsV} protease domain mutations on supporting viral movement was
347 tested in our functional complementation assay using movement-deficient TMV (45, 52).
348 As shown in FIG. 7A, TMVΔCPΔMP-GFP movement was complemented in leaves
349 transiently expressing MP^{CPsV}:RFP as well as in leaves transiently expressing the MP of
350 TMV (MP^{TMV}:RFP) as demonstrated by the occurrence of infection foci at 5 dpai under
351 these conditions. Such efficient functional complementation TMVΔCPΔMP-GFP also
352 occurred in the presence of 34K^{CPsV}:RFP but not by 20K^{CPsV}:RFP. MP^{CPsV}D340A:RFP and
353 MP^{CPsV}D340N:RFP were also able to complement TMVΔCPΔMP-GFP; however, the
354 average sizes of infection foci were smaller than those formed in the presence of
355 MP^{CPsV}:RFP or MP^{TMV}:RFP (FIG. 7B). Interestingly, foci formed in the presence of
356 34K^{CPsV}:RFP, which contains the 30K superfamily domain (45), were larger than the foci
357 formed in the presence MP^{CPsV}:RFP, although they were still smaller than those formed in
358 the presence of MP^{TMV}:RFP (FIG. 7B and 7C). The observation that the expression of the
359 34K^{CPsV} cleavage fragment is sufficient and even more efficient in complementing viral
360 movement than the expression of the full length MP^{CPsV} underscores the importance of
361 efficient MP^{CPsV} cleavage with MP^{CPsV} function in supporting virus movement.

362

363 **34K^{CPsV} behaves as a tubule forming MP**

364 The above-described results indicate that MP^{CPsV} processing into 34 kDa and 20 kDa
365 cleavage products is essential to enable the formation of tubule-like structures at PD and
366 that this feature of MP^{CPsV} contributes to the function as a MP. Given that the expression of
367 the N-terminal 34K^{CPsV} fragment, but not the expression of the C-terminal 20K^{CPsV}
368 fragment, leads to tubule formation at PD and is sufficient for complementing the cell-to-
369 cell movement of a MP-deficient TMV construct, we wondered whether 34K^{CPsV} has the

370 ability to interact with other 34K^{CPsV} molecules as well as with PDLP1, as observed for
371 MP^{CPsV}. FLIM measurements on transiently expressed 34K^{CPsV}:GFP revealed an average
372 GFP fluorescence lifetime of 2,2 ns when this protein was expressed alone (FIG. 8Ai), and
373 a similar value was measured when this protein was co-expressed with PDCB1:Cherry
374 (FIG. 8Aii). However, when 34K^{CPsV}:GFP was co-expressed with 34K^{CPsV}:RFP, the
375 average fluorescence lifetime of GFP was reduced to 1,7 ns, thus revealing a FRET
376 efficiency of 23% (P<0,01). When 34K^{CPsV}:GFP was co-expressed with PDLP1:RFP, the
377 average fluorescence lifetime of GFP was 2,0 ns (FIG. 8Ciii), which represents a FRET
378 efficiency of 9 % (P<0,01). These data indicate that 34K^{CPsV} has the capacity to
379 oligomerize and to interact with PDLP1 similar like the full-length MP^{CPsV}.

380 Finally, we wanted to know whether the formation of tubules by 34K^{CPsV} depends on the
381 ER-Golgi pathway and the targeting of PDLP1 to PD, as in the case of MP^{CPsV}. Co-
382 expression of 34K^{CPsV}:RFP with Sar1:GFP wt (FIG 8Ci, ii and v) allowed the formation of
383 34K^{CPsV}:RFP tubules in 57% of the PD within the observed leaf area (Table 2). On the
384 contrary, when 34K^{CPsV}:RFP was co-expressed with Sar1[H74L]:GFP, 34K^{CPsV}:RFP
385 localized to PD but the percentage of PD with 34K^{CPsV}:RFP tubules was significantly lower
386 (10%, P<0,01; Table 2). The PDLP1:RFP targeting to PD was again inhibited by co-
387 expression of Sar1[H74L]:GFP but not by co-expression of Sar1:GFP, as already shown.
388 Thus, inhibition of ER-Golgi pathway reduces PDLP1 targeting to PD and tubule formation
389 by 34K^{CPsV} and MP^{CPsV}. Both the MP^{CPsV} and its cleavage fragment 34K^{CPsV} interact with
390 PDLP1, which shows reduced targeting to PD upon inhibition of the ER-Golgi pathway.
391 Thus, the 34K^{CPsV} cleavage product carries the PDLP1-interacting and tubule-forming
392 functions required for virus movement and activated upon MP^{CPsV} cleavage.

393

394 **Discussion**

395 We have shown that MP^{CPsV} has the capacity to target PD, to interact at PD with PDLP1 for
396 oligomerization and tubule assembly, and to function in virus movement. Moreover, we
397 found that MP^{CPsV} is cleaved into an N-terminal 34 kD (34K^{CPsV}) fragment carrying the
398 30K super-family domain and into a C-terminal 20 kDa (20K^{CPsV}) fragment carrying an
399 aspartic protease motif responsible for this cleavage. Consistent with the presence of the
400 30K super-family domain, the 34 kDa fragment carries the ability to target PD, to interact

401 with PDLP, and to function in virus movement. Mutations within the catalytic domain of
402 the protease motif abolish tubule formation, alter subcellular localization and decrease the
403 efficiency of the protein in complementing spread of a MP-deficient TMV, thus indicating
404 that the formation of the 34 kDa fragment is a prerequisite for tubule-guided movement.
405 However, the autocleavage-deficient MP^{CPsV}D340A:RFP and MP^{CPsV}D340N:RFP proteins
406 retained some of their movement function and complemented the movement of a MP-
407 deficient TMV construct to some extent without being able to form tubules. This, together
408 with the fact that TMV is the prototype for non-tubule-guided movement, suggests that the
409 tubule-guided mechanism may not be the only mechanism by which MP^{CPsV} supports for
410 virus movement. Nevertheless, tubule-like structures were found at the PD of CPsV-
411 infected sweet orange plants, suggesting that the virus indeed uses a tubule-guided
412 movement as a mechanism for movement in its natural host. Ophiovirus particles have been
413 described as open circular CP decorated flexuous filaments of 3-4 nm thickness (56). Since
414 tubule-forming viruses usually have an icosahedral particle morphology, such as CPMV
415 (15, 37), CaMV (11, 27, 32, 33), GFLV (27, 34-36), alfalfa mosaic virus and brome mosaic
416 virus (39) and tomato spotted wild virus (13), the use of a tubule-guided mechanism by
417 CPsV may be unexpected. Tubule-guided movement by icosahedral viruses depends on
418 CP-MP interactions that may allow the viral particles to be guided along the inner tubule
419 wall (57-60). A tubule-guided mechanism also used by CPsV may therefore be supported
420 by our previous observation that the MP and CP of CPsV are able to interact (46). Based on
421 the importance of the 34K fragment of MP^{CPsV} for virus movement, it may be expected that
422 this fragment interacts with CP within the tubules.

423 Plant virus-encoded proteases belong to three classes (61). Whereas serine and serine-like
424 proteases have been described in *Poty-* (62, 63) and *Secoviridae* (64-66) families, cysteine
425 proteases are present in *Beny-* (67), *Marafi-* (68), *Tymo-* (69) and *Closterovirus* (70), while
426 aspartic proteases occur in the *Caulimoviridae* family (55, 71). The protease of CaMV
427 carries sequence similarity with retrovirus protease (72), thus similar to MP^{CPsV} as shown
428 here. To our knowledge this is the first report of an aspartic protease encoded by a plant
429 virus with a negative-strand RNA genome. Virus-encoded aspartic proteases are small
430 proteins of 10-15 kDa carrying an invariant catalytic aminoacid motif D (T or S) G. The
431 catalytic form of the enzyme is usually composed of two monomers each providing one D

432 (T or S) G motif. Cellular aspartic proteases contain two motifs in a single polypeptide
433 chain (55). The 20K^{CPsV} fragment contains only one DTG motif, which suggested that this
434 fragment should dimerize. As shown here 20K-20K interaction takes place at both the
435 nucleus and cytoplasm. At this latter location 20K^{CPsV} co-localized with the MP^{CPsV}D340A
436 self-cleaving deficient mutant, which is cleaved *in trans* by the 20K^{CPsV} but not when
437 expressed alone. Therefore, the 20K^{CPsV} acts as a viral protease involved in the maturation
438 of the MP^{CPsV} full-length protein. In both transient expression experiments as well as
439 during infection we see that the processing of the full-length MP^{CPsV} is not exhaustive and a
440 high proportion of the MP^{CPsV} remains full length. This is also observed for the trans-
441 cleavage of MP^{CPsV}D340A by 20K^{CPsV}, suggesting that the protease activity is under
442 regulation (61). Mutants at the cleavage site evaluated in this work showed the capacity to
443 undergo autocleavage, even though when the aminoacids ₃₁₀LA₃₁₁ were replaced for
444 residues with different physicochemical properties, suggesting that these positions are not
445 critical for recognition of the cleavage site. Further studies are required to determine the
446 mechanism by which the cleavage site is recognized and cleaved by the protease.
447 Moreover, it would also be important to know whether the 20K^{CPsV} protease targets also
448 other CPsV proteins, or even host proteins, during infection.

449 We recently showed that MP^{CPsV} can suppress RNA silencing (44). It would be interesting
450 to know whether the RNA silencing suppressing activity resides in the N-terminal 20 kDa
451 or 34 kDa cleavage fragment of the protein.

452 In conclusion, we propose here a model where the 54K protein encoded in RNA 2 of CPsV,
453 is a poly-protein containing MP and protease activity and should be renamed hereafter as
454 MP-PRO. The MP-PRO polyprotein is cleaved by its aspartic protease activity. This
455 processing event generates two fragments, an N-terminal fragment (34K^{CPsV}) capable of PD
456 targeting and tubule formation renamed as MP^{CPsV}, and a C-terminal fragment (20K^{CPsV})
457 carrying the aspartic protease activity, renamed as PRO. The MP^{CPsV} fragment is sufficient
458 and even more efficient than the full length MP-PRO in complementing a movement-
459 deficient TMV, although the mechanism can be more specific in the natural host. The
460 observation that the cleavage-deficient mutant MP-PRO D340A supports TMV movement,
461 albeit to a lower efficiency, although it does not form tubules, indicates that the full-length
462 protein complements movement by a different mechanism.

463

464 Material and Methods

465

466 Virus isolates and plant inoculation

467 Young leaves of sweet orange plants [*Citrus sinensis* (L.) Osb] that were either healthy or
468 systemically infected with the CPV-4 isolate of CPsV (73) were used for transmission
469 electron microscopy analysis. The CPsV isolate 90-1-1 (74) was used for mechanical
470 inoculation of *Nicotiana occidentalis* P1 leaves to obtain protein extracts from infected
471 plants for Immunoblot assays.

472

473 Plasmid constructs, bacterial strains and agroinfiltration assays

474 Protein fusions MP^{CPsV}:GFP and MP^{CPsV}:RFP have been described earlier (52). Mutant
475 MP^{CPsV} derivatives D340A, D340N, 20K and 34K were obtained by site-directed
476 mutagenesis with specific primers and Pfu DNA polymerase (Inbio, Argentina), and using
477 the GATEWAY system-based plasmid pTOPO-MP^{CPsV} (46) as template. Primer sequences
478 are available upon request. The PCR products were digested with DpnI (NEB, USA) to
479 remove the methylated DNA template before transformation into *Escherichia coli* DH5 α
480 competent cells. The introduced mutations were verified by DNA sequencing. The resulting
481 pTOPO-MP^{CPsV} derivatives carrying the desired mutations were subjected to LR
482 recombination (ThermoFisher, USA) with destination vectors pB7RWG2 and pB7FWG2
483 (75), and the resulting plasmids that now encode the mutant MP^{CPsV} proteins fused to either
484 RFP or GFP were transferred into *Agrobacterium tumefaciens* GV3101.

485 For transient expression of the fluorescent fusion proteins, *A. tumefaciens* cultures were
486 harvested by centrifugation, resuspended in water to a final OD_{600nm} of 0.3 (unless stated
487 differently) and infiltrated into the abaxial side of the leaf using a syringe without needle.
488 Leaves were observed at 2-3 days post agroinfiltration (dpi). The expression, size and
489 integrity of the fusion proteins were confirmed by Immunoblot assays.

490

491 **Protein analysis**

492 Four leaf discs (1.0 cm in diameter) were excised from *N. benthamiana* leaves expressing
493 the viral proteins, ground in liquid nitrogen to fine powder and resuspended in 200 µl of
494 protein extraction buffer (Tris-HCl 75 mM pH = 6.8, 30% glycerol, 5 % β-
495 mercaptoethanol, 2% SDS, protease complete inhibitor cocktail (Roche, Germany). This
496 extract was centrifuged at 16000 g for 2 min, and the supernatant was used for immunoblot
497 analysis by adding 200 µl of 4X Laemmli buffer. Samples were boiled for 5 min and
498 centrifuged for 2 min at 16000 g. MP^{CpsV} (54 K protein) was detected with anti-54K serum
499 as previously described (52). GFP and RFP fusion proteins were detected with anti-GFP
500 (JL-8) monoclonal antibody (BD Biosciences, Clontech, USA) and anti-RFP (6G6)
501 monoclonal antibody (Chromotek, Germany), respectively. Horseradish peroxidase-
502 conjugated anti-mouse (BioRad, USA) was used as secondary antibody. Chemiluminescent
503 reagent was used for detection of peroxidase activity according to the manufacturer's
504 instructions (GE, ECL Plus Western Blotting Detection Reagents, UK). Densitometry of
505 the protein bands was applied to quantify signal strength using ImageJ(76).

506 **Immunopurification and peptide identification by LC MS/MS**

507 Four grams of tissue powder were resuspended in 8 ml of ice-cold extraction buffer (10
508 mM Tris/HCl pH 7,5; 150 mM NaCl; 5 mM EDTA; 0,5% NP-40, 1mM PMSF)
509 supplemented with one tablet of complete protease inhibitor cocktail (Roche, country) per
510 10 ml of buffer and incubated for 30 min, with occasionally inversion of the tube. This
511 extract was centrifuged at 11000 x g for 30 min, filtered through miracloth paper, and
512 centrifuged again for 30 min at 11000 x g at 4 °C. The cleared extract was incubated with
513 50 µl of GFP-Trap agarose beads (Chromotek, Germany) for 1hr 30 min at 4 °C. The beads
514 were collected by centrifugation at 2500 x g for 2 min at 4 °C. The supernatant was
515 discarded and the beads were washed four times with washing buffer 1 (WB1:10 mM
516 Tris/HCl pH 7,5; 150 mM NaCl; 5 mM EDTA, 1 mM PMSF). Bound proteins were
517 reduced with 50 mM dithiothreitol in 50 mM ammonium bicarbonate and alkylated with 50
518 mM iodoacetamide in ammonium bicarbonate buffer before they were on-bead digested
519 with Tripsin Gold over-night according to manufacture instructions (Promega, USA).
520 Samples were centrifuged at 4 °C and 16000 x g in a microcentrifuge, the supernatants

521 containing the tryptic peptides were desalted with Zip-Tip C18 (Millipore, USA), and
522 samples were lyophilized and finally resuspended in 10 μ l of 0,1% Formic acid solution.

523 The resulting peptides were then separated by reverse phase nanoHPLC (Thermo Scientific,
524 EASY-Spray Accucore (P/N ES801)) with a continuous gradient of two solutions, i.e. 0,1
525 % formic acid in water and 0,1% formic acid in acetonitrile. The nanoHPLC column was
526 coupled to an Electro Spray ionization source (EASY-SPRAY, Thermo Scientific) at a
527 spray voltage of 3,5 kV. Following ionization, the ions were further separated and analyzed
528 by a mass spectrometer Q-Exactive (Thermo Scientific) equipped with a High Collision
529 Dissociation and an Orbitrap analyzer. Protein identification was carried out with
530 MaxQuant 4.0 software, using an *N. benthamiana* database (Boyce Thompson Institute)
531 where the 54K:GFP protein sequence was added. The digestion mode was semispecific to
532 allow identification of the peptides derived from the aspartic protease. All the parameters
533 left were set with the default values. The peptides were analyzed based on MS/MS count,
534 which is the number of sequencing events for this sequence and the Posterior Error
535 Probability (PEP) of the identification. The PEP value essentially operates as a p-value.
536 Peptides with the highest MS/MS count and lowest PEP value were selected.

537

538 **Microscopy**

539 Confocal laser scanning microscopy (CLSM) and Fluorescence lifetime imaging
540 microscopy (FLIM) were performed as described previously (77). Briefly, for CLSM a
541 Leica TCS SP5 II microscope equipped with a HCX PL APO CS 63.0x 1.40 OIL UV
542 objective was used. Excitation/emission wavelengths were 488/524-550 nm for GFP and
543 543/566-634 nm for RFP and 405/473-579nm for Aniline blue. Chloroplast
544 autofluorescence was detected by excitation at 488 nm and emission filtering at 654-
545 730nm. Images were acquired with LAS AF version 2.2.1 4842 software and processed
546 with ImageJ software. Callose staining was achieved by infiltrating leaf disks with 0,01%
547 Methyl blue (Fluka, UK) solution in PBS buffer prior to observation. FLIM analysis of GFP
548 fluorescence was done with a Lambert Instruments Fluorescence Lifetime Attachment
549 (LIFA) mounted on a Nikon TE2000 inverted microscope. The microscope was equipped
550 with a 63x NA 1.4 oil objective and specific filters for excitation/emission wavelengths of

551 460–500/510–560 nm for detection of GFP and of 550–600/615–665 nm for detection of
552 RFP. FLIM images were acquired and processed with LI-FLIM software version 1.2.9.117
553 (Lambert Instruments). ANOVA analysis was performed, followed by a Turkey test ($\alpha=$
554 0.01). FRET efficiency was calculated as $\%FRET = 1 - \tau_{DA} / \tau_D \times 100$, whereby τ_D is the
555 lifetime of the donor in the absence of the acceptor and τ_{DA} is the lifetime of the donor in
556 the presence of the acceptor.

557 For transmission electron microscopy (TEM), symptomatic leaves from systemically
558 infected sweet orange plants and healthy leaves from non-infected plants were harvested at
559 a similar developmental stage and fixed at 4 °C with 2% glutaraldehyde in phosphate buffer
560 under smooth vacuum during 2 hrs. Secondary fixation was carried out at 4 °C with 1%
561 osmium tetroxide under vacuum for 1 hr. Samples were dehydrated and embedded in epoxy
562 resin followed by ultrathin sectioning (70 nm). Uranyl acetate and lead citrate were used to
563 contrast the samples prior to observation with a JEM 1200 EX II transmission electron
564 microscope (JEOL Ltd., Tokyo, Japan). Images were acquired with an Erlangshen
565 ES1000W (Model 785) CCD camera (Gatan Inc., Pleasanton, California, USA).

566

567 **TMV *trans*-complementation assays**

568 Trans-complementation assays were performed as previously described (45). Briefly,
569 agrobacteria cultures carrying a TMV Δ MP Δ CP-GFP-expressing binary plasmid were
570 resuspended in water to an OD_{600nm} of 1×10^{-5} and infiltrated into *N. benthamiana* leaves
571 together with agrobacteria resuspended in water to an OD_{600nm} of 0.3 and carrying plasmids
572 encoding either RFP, MP^{TMV}, MP^{CPsV}, MP^{CPsV}D340A, MP^{CPsV}D340N, 34K^{CPsV}, or 20K^{CPsV}.
573 The development of infection foci was observed at 3, 4, and 5 dpai. At these time points,
574 scaled images were acquired and the size of the infection foci was measured with ImageJ
575 software (76).

576

577 **Acknowledgments**

578 This work was performed with financial support of ANPCyT and CONICET (grant
579 PICT2014-2202, PIP 0847 and PICS D498/16) in Argentina and with financial support
580 through CNRS PICS 06702 and an EMBO short-term fellowship (to GRL) in France.,

581 France. We would like to thank Dr. Susana Jurado and Dr. Roxana Peralta for their
582 technical assistance with TEM sample preparations conducted at the Servicio Central de
583 Microscopía Electrónica, Fac. Ciencias Veterinarias-UNLP and to Dra. Pía Valacco from
584 the Centro de Estudios Químicos y Biológicos por Espectrometría de Masa (CEQUIBIEM,
585 UBA) for help with the proteomic analysis. We are also grateful for support by Jérôme
586 Mutterer (IBMP, Strasbourg) in performing FLIM measurements. Author Contributions:
587 Conceived and designed the experiments: GRL, EJP, MLG, MH. Performed the
588 experiments: GRL, MBB, EJP. Analyzed the data: GRL, EJP, MBB. Contributed
589 reagents/materials/analysis tools: MLG, MH. Wrote the paper: GRL, EJP, MLG, MH.

590 **Figure legends**

591 **FIG. 1. Tubule-like structures in the cell walls of CPsV-infected *C. sinensis* plants.** (A)
592 Transmission electron microscopy images showing PD in healthy (i) and infected (ii) *C.*
593 *sinensis* plants. PD, plasmodesmata; CW, cell wall. The arrow in (ii) points to a tubule-like
594 structure protruding from a modified PD. Scale bar, 100 nm. (B) CLSM of *N. benthamiana*
595 epidermal cells expressing GFP:MP^{CPsV} (i) or MP^{CPsV}:GFP (ii). Arrowheads in (i) and (ii)
596 indicate the presence of GFP:MP^{CPsV} and MP^{CPsV}:GFP at PD; arrows in (ii) indicate the
597 presence of tubules containing MP^{CPsV}:GFP at PD. Scale bar, 30µm.

598 **FIG.2. MP^{CPsV}-PDL1 interaction is necessary for MP-tubule formation at PD.** (A)
599 FRET-FLIM measurements of *N. benthamiana* epidermal cells expressing (i) MP^{CPsV}:GFP
600 alone, or together with either (ii) PDCB1:Cherry, (iii) MP^{CPsV}:RFP, or (iv) PDL1:RFP.
601 Fluorescent intensity images (top) are combined with fluorescence lifetime images (bottom)
602 showing lifetime in false color code according to the color scale on the left. Scale bar, 10
603 µm. A representative fluorescence lifetime analysis based on three independent replicate
604 experiments is shown (v). τ, fluorescent lifetime (ns); SD, standard deviation; N, number of
605 cells analyzed. Asterisks represent significant differences compared to MP^{CPsV}:GFP
606 expressed alone (P<0,01). (B) FRET-FLIM measurements of *N. benthamiana* expressing (i)
607 GFP:MP^{CPsV} alone or together with (ii) PDCB1:Cherry, (iii) MP^{CPsV}:RFP, or (iv)
608 PDL1:RFP. Fluorescent intensity images (top) are combined with fluorescence lifetime
609 images (bottom) showing lifetime in false color code according to the color scale on the
610 left. Scale bar, 10 µm. A representative fluorescence lifetime analysis based on three
611 independent replicate experiments is shown (v). τ, fluorescent lifetime (ns); SD, standard

612 deviation; N, number of cells analyzed. Asterisks represent significant differences respect
 613 to GFP:MP^{CPsV} expressed alone in GFP fluorescence lifetime (P<0,01). (C) Expression of
 614 PDLP1:RFP together with either Sar1:GFP (i and ii) or Sar1[H74L]:GFP (iii and iv) (only
 615 RFP channel is shown in magenta). The images (ii) and (iv) (scale bar, 10 μ m) show
 616 enlargements of the framed tissue regions indicated in (i) and (ii) (scale bar, 50 μ m);
 617 arrowheads indicate PD. Immunoblots (v) show protein expression levels in each
 618 experiment. (D) Expression of MP^{CPsV}:RFP together with either Sar1:GFP (i and ii) or
 619 Sar1[H74L]:GFP (iii and iv). RFP channel is shown in magenta and callose staining is
 620 showed in yellow. The images (ii) and (iv) (scale bar, 5 μ m) show enlargements of the
 621 framed tissue regions indicated in (i) and (ii) (scale bar, 10 μ m); arrowheads indicate PD;
 622 arrows indicate tubule-like structures at PD. Immunoblots (v) show protein expression
 623 levels in each experiment

624 **FIG.3. Fluorescence protein orientation affects MP^{CPsV} movement activity and**
 625 **cleavage.** (A) (Left) Representative images of *N. benthamiana* leaves showing the
 626 development of TMV Δ CP Δ MP-GFP infection foci at 5 dpai in the presence of either
 627 GFP:MP^{CPsV}, MP^{CPsV}:GFP or GFP (negative control). Scale bar, 10 mm. (Right) Analysis
 628 of the sizes of infection foci shown in (A). Letters above columns indicate statistical
 629 differences (P<0,01). (B) Immunoblot with anti-GFP antibody. The upper band corresponds
 630 to the full-length fusion protein; asterisks indicate the presence of additional GFP-
 631 containing proteins. Molecular masses are indicated on the right of the immunoblot. (C)
 632 (Top) Schematic representation of the predicted chloroplast transit peptide (cTP) at the N-
 633 terminal end of MP^{CPsV}; (bottom) subcellular localization of MP^{CPsV}:GFP (upper panel
 634 yellow) and GFP:MP^{CPsV} (lower panel yellow) in relation to the chloroplasts
 635 (autofluorescence, in red). Scale bar, 10 μ m.

636 **FIG. 4. MP^{CPsV} encodes an aspartic protease motif.** (A) Immunoblot analysis of healthy
 637 and CPsV infected *N. occidentalis* P1 plants using anti-MP^{CPsV} (anti-54) serum. Molecular
 638 masses of virus-specific bands are indicated on the right of the immunoblot. (B) (i) (Top)
 639 Representation of part of the aminoacids sequence of the MP^{CPsV} aligning the aspartic
 640 protease domain with the respective domains in Cathepsin D (PDB structure ID: [4Od9_A](#))
 641 and HIV-2 protease (PDB structure ID: [3ec0_A](#)), the catalytic D residue is underlined in

642 each case. (Bottom) Alignment of the aminoacid sequences of HIV protease substrate
 643 peptides against the aminoacid sequence of MP^{CPsV}. The specific HIV protease cleavage
 644 releases specific proteins; MA, matrix; CA, capsid; NC, nucleocapsid; TF, trans-frame
 645 peptide; PR, protease; AutoP, auto proteolysis site; RT, reverse transcriptase; RH, RNase
 646 H; IN, integrase. Cleavage site is indicated with an “[”. (ii and iii) Representation of part of
 647 the aminoacids sequence of the MP^{MiLBVV} and MP^{BLMaV} respectively, aligning the aspartic
 648 protease domain with the respective domains in Cathepsin D (PDB structure ID: [4Od9_A](#))
 649 and aspartic protease (PDB structure ID: [3LIY_D](#)). The catalytic D residue is underlined.
 650 (C) MS/MS spectra showing the ions matching with 54K derived peptides indicated at the
 651 bottom of each spectra. (i) Spectra of the peptide KSVSINLSNFL corresponding to the C-
 652 terminal end of the 34K fragment and (ii), spectra of the peptide ADQRRAPPPPQLEKR
 653 corresponding to the N-terminal end of the 20K protein. MS/MS counts and PEP values are
 654 indicated. (D) MP^{CPsV} mutants used in this work. Aminoacid replacements are indicated
 655 underlined. (E) Immunoblot of protein extracts of *N. benthamiana* tissues transiently
 656 expressing either RFP, MP^{CPsV}:RFP, MP^{CPsV}D340A:RFP, MP^{CPsV}D340N:RFP,
 657 34K^{CPsV}:RFP, 20K^{CPsV}:RFP, MP^{CPsV}L310D:RFP, MP^{CPsV}A311D:RFP, MP^{CPsV}A311R:RFP
 658 or MP^{CPsV}A311H:RFP with anti-RFP monoclonal antibody. Molecular masses are indicated
 659 on the left of the immunoblot.

660 **FIG. 5. Subcellular localizations of MP^{CPsV} mutants.** Co-expression of PDCB1:Cherry
 661 with together with (A) MP^{CPsV}:GFP, (B) MP^{CPsV}D340A:GFP, (C) MP^{CPsV}D340N:GFP (D)
 662 34K^{CPsV}:GFP or (E) 20K^{CPsV}:GFP in *N. benthamiana* epidermal cells at 3 dpi. The patterns
 663 of GFP fluorescence (yellow), Cherry fluorescence (magenta), and chloroplast
 664 autofluorescence (red) are shown. Arrows indicate locations of tubule-like structures at PD;
 665 arrowheads GFP-fluorescent PD without tubules; white rectangles, chloroplasts; Nu,
 666 nucleus. Scale bar, 20 μ m.

667 **FIG. 6. 20K^{CPsV} cleavage product retains the aspartic protease activity.**(A) FRET-FLIM
 668 measurements of *N. benthamiana* epidermal cells expressing (i) 20K^{CPsV}:GFP either alone
 669 or together with (ii) RFP or (iii) 20K^{CPsV}:RFP. Fluorescent intensity images (top) are
 670 combined with fluorescence lifetime images (bottom) showing lifetime in false color code
 671 according to the color scale on the left. Scale bar, 10 μ m. A representative fluorescence

672 lifetime analysis based on two independent replicate experiments is shown (iv and v), in
673 which the lifetime was measured in the nucleus (iv) and cytoplasm (v). τ , fluorescent
674 lifetime (ns); SD, standard deviation; N, number of nucleus or cytoplasm analyzed.
675 Asterisks represent significant differences compared to 20K^{CPsV}:GFP expressed alone
676 ($P < 0.01$). (B) Immunoblot analysis of *N. benthamiana* plants expressing
677 MP^{CPsV}D340A:GFP either alone or in combination with MP^{CPsV}:RFP or 20K^{CPsV}:RFP. Top
678 panel, anti-RFP antibody; bottom panel, anti-GFP antibody. Arrows indicate the fragment
679 produced by *in trans* proteolytic processing of MP^{CPsV}D340A:GFP by either MP^{CPsV}:RFP
680 (left) or 20K^{CPsV}:RFP (right). (C) Expression of MP^{CPsV}D340A:GFP (yellow) together with
681 (i) MP^{CPsV}:RFP (magenta) or (ii) with 20K^{CPsV}:RFP (magenta) in *N. benthamiana* leaves at
682 3 dpai. Arrowheads indicate tubule-like structures at PD. Scale bar, 10 μ m.

683 **FIG. 7. Virus movement activity of MP^{CPsV} mutants.** (A) Representative images
684 showing TMV Δ CP Δ MP-GFP infection foci at 5 dpai in *N. benthamiana* leaves expressing
685 the indicated protein. Scale bar, 10 mm. (B) Size of infection foci in the presence of
686 indicated proteins measured at 5 dpai. Each letter indicates protein treatments with
687 statistical differences between them ($P < 0.01$). (C) Size distribution of the infection foci
688 according to specific treatment at 5 dpai.

689 **FIG. 8. 34K^{CPsV}-PDLP interaction is necessary for tubule formation at PD.** A) FRET-
690 FLIM measurements of *N. benthamiana* epidermal cells expressing (i) 34K^{CPsV}:GFP either
691 alone, or together with (ii) PDCB1:Cherry, (iii) 34K^{CPsV}:RFP, or (iv) PDLP1:RFP.
692 Fluorescent intensity images (top) are combined with GFP fluorescence lifetime images
693 (bottom) indicating lifetime in false color code according to the scale on the left. Scale bar,
694 10 μ m. Lifetime analysis (v): τ , fluorescent lifetime (ns); SD, standard deviation; n, number
695 of cells analyzed. Asterisks represent a significant reduction in GFP fluorescence lifetime
696 ($P < 0.01$) compared to 34K^{CPsV}:GFP. (B) Expression of 34K^{CPsV}:RFP together with
697 Sar1:GFP (i and ii) or with Sar1[H74L]:GFP (iii and iv). RFP channel is shown in magenta
698 and callose staining is showed in yellow. The images (ii) and (iv) (scale bar, 5 μ m) are
699 enlargements of the framed leaf regions shown in (i) and (ii) (scale bar, 10 μ m);
700 arrowheads, PD; arrows, tubule-like structures at PD. Immunoblot analysis showing protein
701 expression levels (v).

702

703 References

- 704 1. **Lucas WJ.** 2006. Plant viral movement proteins: agents for cell-to-cell trafficking of viral genomes.
705 *Virology* **344**:169-184.
- 706 2. **Taliansky M, Torrance L, Kalinina NO.** 2008. Role of plant virus movement proteins. *Methods*
707 *Mol Biol* **451**:33-54.
- 708 3. **Benitez-Alfonso Y, Cantrill L, Jackson D.** 2006. Plasmodesmata: Cell-Cell Channels in Plants, p
709 101-112, *Cell-Cell Channels*. Springer New York, New York, NY.
- 710 4. **Esau K, Thorsch J.** 1985. Sieve plate pores and plasmodesmata, the communication channels of the
711 cytoplasm: ultrastructural aspects and developmental relations. *Am J Bot* **72**:1641-1653.
- 712 5. **Tilsner J, Nicolas W, Rosado A, Bayer EM.** 2016. Staying Tight: Plasmodesmal Membrane
713 Contact Sites and the Control of Cell-to-Cell Connectivity in Plants. *Annu Rev Plant Biol* **67**:337-
714 364.
- 715 6. **De Storme N, Geelen D.** 2014. Callose homeostasis at plasmodesmata: molecular regulators and
716 developmental relevance. *Frontiers in Plant Science* **5**:1-23.
- 717 7. **Heinlein M, Epel BL.** 2004. Macromolecular Transport and Signaling Through Plasmodesmata, p
718 93-164, *International Review of Cytology*, vol 235. Academic Press.
- 719 8. **Zavaliev R, Ueki S, Epel BL, Citovsky V.** 2011. Biology of callose (beta-1,3-glucan) turnover at
720 plasmodesmata. *Protoplasma* **248**:117-130.
- 721 9. **Niehl A, Heinlein M.** 2011. Cellular pathways for viral transport through plasmodesmata.
722 *Protoplasma* **248**:75-99.
- 723 10. **Pitzalis N, Heinlein M.** 2017. The roles of membranes and associated cytoskeleton in plant virus
724 replication and cell-to-cell movement. *J Exp Bot* **69**:117-132.
- 725 11. **Perbal MC, Thomas CL, Maule AJ.** 1993. Cauliflower mosaic virus gene I product (P1) forms
726 tubular structures which extend from the surface of infected protoplasts. *Virology* **195**:281-285.
- 727 12. **Ritzenthaler C, Schmit A-C, Michler P, Stussi-Garaud C, Pinck L.** 1995. Grapevine fanleaf
728 nepovirus putative movement protein is involved in tubule formation in vivo. *Mol Plant Microbe*
729 *Interact* **8**:379-387.
- 730 13. **Storms MM, Kormelink R, Peters D, Van Lent JW, Goldbach RW.** 1995. The nonstructural
731 NSm protein of tomato spotted wilt virus induces tubular structures in plant and insect cells.
732 *Virology* **214**:485-493.
- 733 14. **van der Wel NN, Goldbach RW, van Lent JW.** 1998. The movement protein and coat protein of
734 alfalfa mosaic virus accumulate in structurally modified plasmodesmata. *Virology* **244**:322-329.
- 735 15. **van Lent J, Storms M, van der Meer F, Wellink J, Goldbach R.** 1991. Tubular structures
736 involved in movement of cowpea mosaic virus are also formed in infected cowpea protoplasts.
737 *Journal of General Virology* **72**:2615-2623.
- 738 16. **Wieczorek A, Sanfacon H.** 1993. Characterization and subcellular localization of tomato ringspot
739 nepovirus putative movement protein. *Virology* **194**:734-742.
- 740 17. **Peña E, Niehl A, Heinlein M.** 2012. Viral Studies Point the Way: Mechanisms of Intercellular
741 Transport, p 1-43. *In* Kragler F, Hülskamp M (ed), *Short and Long Distance Signaling*. Springer
742 New York, New York, NY.
- 743 18. **Amari K, Di Donato M, Dolja VV, Heinlein M.** 2014. Myosins VIII and XI Play Distinct Roles in
744 Reproduction and Transport of Tobacco Mosaic Virus. *PLOS Pathogens* **10**:e1004448.
- 745 19. **Guenoune-Gelbart D, Elbaum M, Sagi G, Levy A, Epel BL.** 2008. Tobacco mosaic virus (TMV)
746 replicase and movement protein function synergistically in facilitating TMV spread by lateral
747 diffusion in the plasmodesmal desmotubule of *Nicotiana benthamiana*. *Mol Plant Microbe Interact*
748 **21**:335-345.
- 749 20. **Boyko V, Hu Q, Seemanpillai M, Ashby J, Heinlein M.** 2007. Validation of microtubule-
750 associated Tobacco mosaic virus RNA movement and involvement of microtubule-aligned particle
751 trafficking. *Plant J* **51**:589-603.
- 752 21. **Niehl A, Peña EJ, Amari K, Heinlein M.** 2013. Microtubules in viral replication and transport.
753 *Plant J* **75**:290-308.

- 754 22. **Sambade A, Brandner K, Hofmann C, Seemanpillai M, Mutterer J, Heinlein M.** 2008.
755 Transport of TMV movement protein particles associated with the targeting of RNA to
756 plasmodesmata. *Traffic* **9**:2073-2088.
- 757 23. **Su S, Liu Z, Chen C, Zhang Y, Wang X, Zhu L, Miao L, Wang XC, Yuan M.** 2010. Cucumber
758 mosaic virus movement protein severs actin filaments to increase the plasmodesmal size exclusion
759 limit in tobacco. *Plant Cell* **22**:1373-1387.
- 760 24. **Lewis JD, Lazarowitz SG.** 2010. Arabidopsis synaptotagmin SYTA regulates endocytosis and virus
761 movement protein cell-to-cell transport. *Proc Natl Acad Sci U S A* **107**:2491-2496.
- 762 25. **Levy A, Zheng JY, Lazarowitz SG.** 2015. Synaptotagmin SYTA forms ER-plasma membrane
763 junctions that are recruited to plasmodesmata for plant virus movement. *Current biology : CB*
764 **25**:2018-2025.
- 765 26. **Uchiyama A, Shimada-Beltran H, Levy A, Zheng JY, Javia PA, Lazarowitz SG.** 2014. The
766 Arabidopsis synaptotagmin SYTA regulates the cell-to-cell movement of diverse plant viruses. *Front*
767 *Plant Sci* **5**:584.
- 768 27. **Amari K, Boutant E, Hofmann C, Schmitt-Keichinger C, Fernandez-Calvino L, Didier P,**
769 **Lerich A, Mutterer J, Thomas CL, Heinlein M, Mely Y, Maule AJ, Ritzenthaler C.** 2010. A
770 family of plasmodesmal proteins with receptor-like properties for plant viral movement proteins.
771 *PLoS Pathog* **6**:e1001119.
- 772 28. **den Hollander PW, Kieper SN, Borst JW, van Lent JW.** 2016. The role of plasmodesma-located
773 proteins in tubule-guided virus transport is limited to the plasmodesmata. *Arch Virol* **161**:2431-2440.
- 774 29. **Thomas CL, Bayer EM, Ritzenthaler C, Fernandez-Calvino L, Maule AJ.** 2008. Specific
775 targeting of a plasmodesmal protein affecting cell-to-cell communication. *PLoS Biol* **6**:e7.
- 776 30. **Carluccio AV, Stabolone L.** 2014. Interference of Brefeldin A in viral movement protein tubules
777 assembly. *Plant Signal Behav* **9**:e29121.
- 778 31. **Huang Z, Han Y, Howell SH.** 2000. Formation of Surface Tubules and Fluorescent Foci in
779 Arabidopsis thaliana Protoplasts Expressing a Fusion between the Green Fluorescent Protein and the
780 Cauliflower Mosaic Virus Movement Protein. *Virology* **271**:58-64.
- 781 32. **Cheng CP, Tzafrir I, Lockhart BE, Olszewski NE.** 1998. Tubules containing virions are present in
782 plant tissues infected with Commelina yellow mottle badnavirus. *J Gen Virol* **79**:925-929.
- 783 33. **Kitajima EW, Lauritis JA, Swift H.** 1969. Fine structure of zinnial leaf tissues infected with dahlia
784 mosaic virus. *Virology* **39**:240-249.
- 785 34. **Amari K, Lerich A, Schmitt-Keichinger C, Dolja VV, Ritzenthaler C.** 2011. Tubule-guided cell-
786 to-cell movement of a plant virus requires class XI myosin motors. *PLoS Pathog* **7**:e1002327.
- 787 35. **Laporte C, Vetter G, Loudes AM, Robinson DG, Hillmer S, Stussi-Garaud C, Ritzenthaler C.**
788 2003. Involvement of the secretory pathway and the cytoskeleton in intracellular targeting and tubule
789 assembly of Grapevine fanleaf virus movement protein in tobacco BY-2 cells. *Plant Cell* **15**:2058-
790 2075.
- 791 36. **Pouwels J, Van Der Krogt GN, Van Lent J, Bisseling T, Wellink J.** 2002. The cytoskeleton and
792 the secretory pathway are not involved in targeting the Cowpea mosaic virus movement protein to
793 the cell periphery. *Virology* **297**:48-56.
- 794 37. **Wellink J, van Lent JW, Verver J, Sijen T, Goldbach RW, van Kammen A.** 1993. The cowpea
795 mosaic virus M RNA-encoded 48-kilodalton protein is responsible for induction of tubular structures
796 in protoplasts. *J Virol* **67**:3660-3664.
- 797 38. **Kormelink R, Storms M, Van Lent J, Peters D, Goldbach R.** 1994. Expression and subcellular
798 location of the NSM protein of tomato spotted wilt virus (TSWV), a putative viral movement
799 protein. *Virology* **200**:56-65.
- 800 39. **Kasteel DT, van der Wel NN, Jansen KA, Goldbach RW, van Lent JW.** 1997. Tubule-forming
801 capacity of the movement proteins of alfalfa mosaic virus and brome mosaic virus. *J Gen Virol* **78** (
802 **Pt 8**):2089-2093.
- 803 40. **Garcia ML, Bo ED, da Graça JV, Gago-Zachert S, Hammond J, Moreno P, Natsuaki T, Pallas**
804 **V, Navarro JA, Reyes CA, Luna GR, Sasaya T, Tzanetakis IE, Vaira AM, Verbeek M, Ictv**
805 **Report C.** 2017. ICTV Virus Taxonomy Profile: Ophioviridae. *J Gen Virol* **98**:1161-1162.
- 806 41. **García ML, Bó ED, da Graça JV, Gago-Zachert S, Hammond J, Moreno P, Natsuaki T, Pallas**
807 **V, Navarro JA, Reyes CA, Luna GR, Sasaya T, Tzanetakis IE, Vaira AM, Verbeek M,**
808 **Consortium IR.** 2018. Corrigendum: ICTV Virus Taxonomy Profile: Ophioviridae. *Journal of*
809 *General Virology* **99**:949-949.

- 810 42. **Naum-Ongania G, Gago-Zachert S, Pena E, Grau O, Garcia ML.** 2003. Citrus psorosis virus
811 RNA 1 is of negative polarity and potentially encodes in its complementary strand a 24K protein of
812 unknown function and 280K putative RNA dependent RNA polymerase. *Virus Res* **96**:49-61.
- 813 43. **Reyes CA, Ocolotobiche EE, Marmisolle FE, Robles Luna G, Borniego MB, Bazzini AA,**
814 **Asurmendi S, Garcia ML.** 2016. Citrus psorosis virus 24K protein interacts with citrus miRNA
815 precursors, affects their processing and subsequent miRNA accumulation and target expression. *Mol*
816 *Plant Pathol* **17**:317-329.
- 817 44. **Robles Luna G, Reyes CA, Pena EJ, Ocolotobiche E, Baeza C, Borniego MB, Kormelink R,**
818 **Garcia ML.** 2017. Identification and characterization of two RNA silencing suppressors encoded by
819 ophioviruses. *Virus Res* **235**:96-105.
- 820 45. **Borniego MB, Karlin D, Pena EJ, Robles Luna G, Garcia ML.** 2016. Bioinformatic and
821 mutational analysis of ophiovirus movement proteins, belonging to the 30K superfamily. *Virology*
822 **498**:172-180.
- 823 46. **Robles Luna G, Peña EJ, Borniego MB, Heinlein M, Garcia ML.** 2013. Ophioviruses CPsV and
824 MiLBVV movement protein is encoded in RNA 2 and interacts with the coat protein. *Virology*
825 **441**:152-161.
- 826 47. **Sánchez de la Torre E, Riva O, Zandomeni R, Grau O, García ML.** 1998. The top component of
827 Citrus psorosis virus contains two ssRNAs, the smaller encodes the coat protein. *Molecular Plant*
828 *Pathology On-Line*.
- 829 48. **Simpson C, Thomas C, Findlay K, Bayer E, Maule AJ.** 2009. An Arabidopsis GPI-anchor
830 plasmodesmal neck protein with callose binding activity and potential to regulate cell-to-cell
831 trafficking. *Plant Cell* **21**:581-594.
- 832 49. **Robinson DG, Herranz M-C, Bubeck J, Pepperkok R, Ritzenthaler C.** 2007. Membrane
833 Dynamics in the Early Secretory Pathway. *Critical Reviews in Plant Sciences* **26**:199-225.
- 834 50. **Takeuchi M, Ueda T, Sato K, Abe H, Nagata T, Nakano A.** 2000. A dominant negative mutant of
835 sar1 GTPase inhibits protein transport from the endoplasmic reticulum to the Golgi apparatus in
836 tobacco and Arabidopsis cultured cells. *Plant J* **23**:517-525.
- 837 51. **Emanuelsson O, Nielsen H, Brunak S, von Heijne G.** 2000. Predicting subcellular localization of
838 proteins based on their N-terminal amino acid sequence. *J Mol Biol* **300**:1005-1016.
- 839 52. **Robles Luna G, Peña EJ, Borniego MB, Heinlein M, Garcia ML.** 2013. Ophioviruses CPsV and
840 MiLBVV movement protein is encoded in RNA 2 and interacts with the coat protein. *Virology*
841 **441**:152-161.
- 842 53. **Soding J, Biegert A, Lupas AN.** 2005. The HHpred interactive server for protein homology
843 detection and structure prediction. *Nucleic Acids Res* **33**:W244-248.
- 844 54. **Prabu-Jeyabalan M, Nalivaika E, Schiffer CA.** 2002. Substrate shape determines specificity of
845 recognition for HIV-1 protease: analysis of crystal structures of six substrate complexes. *Structure*
846 **10**:369-381.
- 847 55. **Rawlings ND, Barrett AJ.** 2004. 1 - Introduction: aspartic peptidases and their clans, p 3-12,
848 *Handbook of Proteolytic Enzymes (Second Edition)*. Academic Press, London.
- 849 56. **Garcia ML, Dal Bo E, Grau O, Milne RG.** 1994. The closely related citrus ringspot and citrus
850 psorosis viruses have particles of novel filamentous morphology. *J Gen Virol* **75**:3585-3590.
- 851 57. **Belin C, Schmitt C, Gaire F, Walter B, Demangeat G, Pinck L.** 1999. The nine C-terminal
852 residues of the grapevine fanleaf nepovirus movement protein are critical for systemic virus spread. *J*
853 *Gen Virol* **80 (Pt 6)**:1347-1356.
- 854 58. **Carvalho CM, Wellink J, Ribeiro SG, Goldbach RW, Van Lent JW.** 2003. The C-terminal
855 region of the movement protein of Cowpea mosaic virus is involved in binding to the large but not to
856 the small coat protein. *J Gen Virol* **84**:2271-2277.
- 857 59. **Lekkerkerker A, Wellink J, Yuan P, van Lent J, Goldbach R, van Kammen AB.** 1996. Distinct
858 functional domains in the cowpea mosaic virus movement protein. *J Virol* **70**:5658-5661.
- 859 60. **Thomas CL, Maule AJ.** 1995. Identification of structural domains within the cauliflower mosaic
860 virus movement protein by scanning deletion mutagenesis and epitope tagging. *The Plant Cell*
861 **7**:561-572.
- 862 61. **Rodamilans B, Shan H, Pasin F, Garcia JA.** 2018. Plant Viral Proteases: Beyond the Role of
863 Peptide Cutters. *Front Plant Sci* **9**:666.
- 864 62. **Riechmann JL, Lain S, Garcia JA.** 1992. Highlights and prospects of potyvirus molecular biology.
865 *J Gen Virol* **73**:1-16.

- 866 63. **Carrington JC, Dougherty WG.** 1987. Small nuclear inclusion protein encoded by a plant
867 potyvirus genome is a protease. *J Virol* **61**:2540-2548.
- 868 64. **Margis R, Viry M, Pinck M, Pinck L.** 1991. Cloning and in vitro characterization of the grapevine
869 fanleaf virus proteinase cistron. *Virology* **185**:779-787.
- 870 65. **Reddick BB, Habera LF, Law MD.** 1997. Nucleotide sequence and taxonomy of maize chlorotic
871 dwarf virus within the family Sequiviridae. *J Gen Virol* **78**:1165-1174.
- 872 66. **Turnbull-Ross AD, Mayo MA, Reavy B, Murrant AF.** 1993. Sequence analysis of the parsnip
873 yellow fleck virus polyprotein: evidence of affinities with picornaviruses. *J Gen Virol* **74**:555-561.
- 874 67. **Hehn A, Fritsch C, Richards KE, Guilley H, Jonard G.** 1997. Evidence for in vitro and in vivo
875 autocatalytic processing of the primary translation product of beet necrotic yellow vein virus RNA 1
876 by a papain-like proteinase. *Arch Virol* **142**:1051-1058.
- 877 68. **Hammond RW, Ramirez P.** 2001. Molecular characterization of the genome of Maize rayado fino
878 virus, the type member of the genus Marafivirus. *Virology* **282**:338-347.
- 879 69. **Bransom KL, Dreher TW.** 1994. Identification of the essential cysteine and histidine residues of
880 the turnip yellow mosaic virus protease. *Virology* **198**:148-154.
- 881 70. **Agranovsky AA, Koonin EV, Boyko VP, Maiss E, Frotschl R, Lunina NA, Atabekov JG.** 1994.
882 Beet yellows closterovirus: complete genome structure and identification of a leader papain-like thiol
883 protease. *Virology* **198**:311-324.
- 884 71. **Hull R.** 2014. Chapter 6 - Genome Composition, Organization, and Expression, p 247-339, *Plant*
885 *Virology* (Fifth Edition). Academic Press, Boston.
- 886 72. **Torruella M, Gordon K, Hohn T.** 1989. Cauliflower mosaic virus produces an aspartic proteinase
887 to cleave its polyproteins. *EMBO J* **8**:2819-2825.
- 888 73. **Garnsey SM, Timmer LW.** Mechanical transmissibility of Citrus ringspot virus isolates from
889 Florida, Texas, and California. , p 174-179. *In* Calavan EC, Garnsey SM, Timmer LW (ed),
890 International Organization of Citrus Virologists c/o Department of Plant Pathology University of
891 California, Riverside, USA.
- 892 74. **García ML, Derrick KS, Grau O.** Citrus psorosis associated virus and citrus ringspot virus belong
893 to a new virus group, p 430-431. *In* P. Moreno JvdGaLWT (ed), IOCV,
- 894 75. **Karimi M, Inze D, Depicker A.** 2002. GATEWAY vectors for Agrobacterium-mediated plant
895 transformation. *Trends Plant Sci* **7**:193-195.
- 896 76. **Schneider CA, Rasband WS, Eliceiri KW.** 2012. NIH Image to ImageJ: 25 years of image
897 analysis. *Nat Methods* **9**:671-675.
- 898 77. **Peña EJ, Robles Luna G, Zaneck MC, Borniego MB, Reyes CA, Heinlein M, Garcia ML.** 2012.
899 Citrus psorosis and Mirafiori lettuce big-vein ophiovirus coat proteins localize to the cytoplasm and
900 self interact in vivo. *Virus Res* **170**:34-43.
- 901
- 902

TABLE 1. MP^{CPsV} tubule formation upon inhibition of the secretory pathway

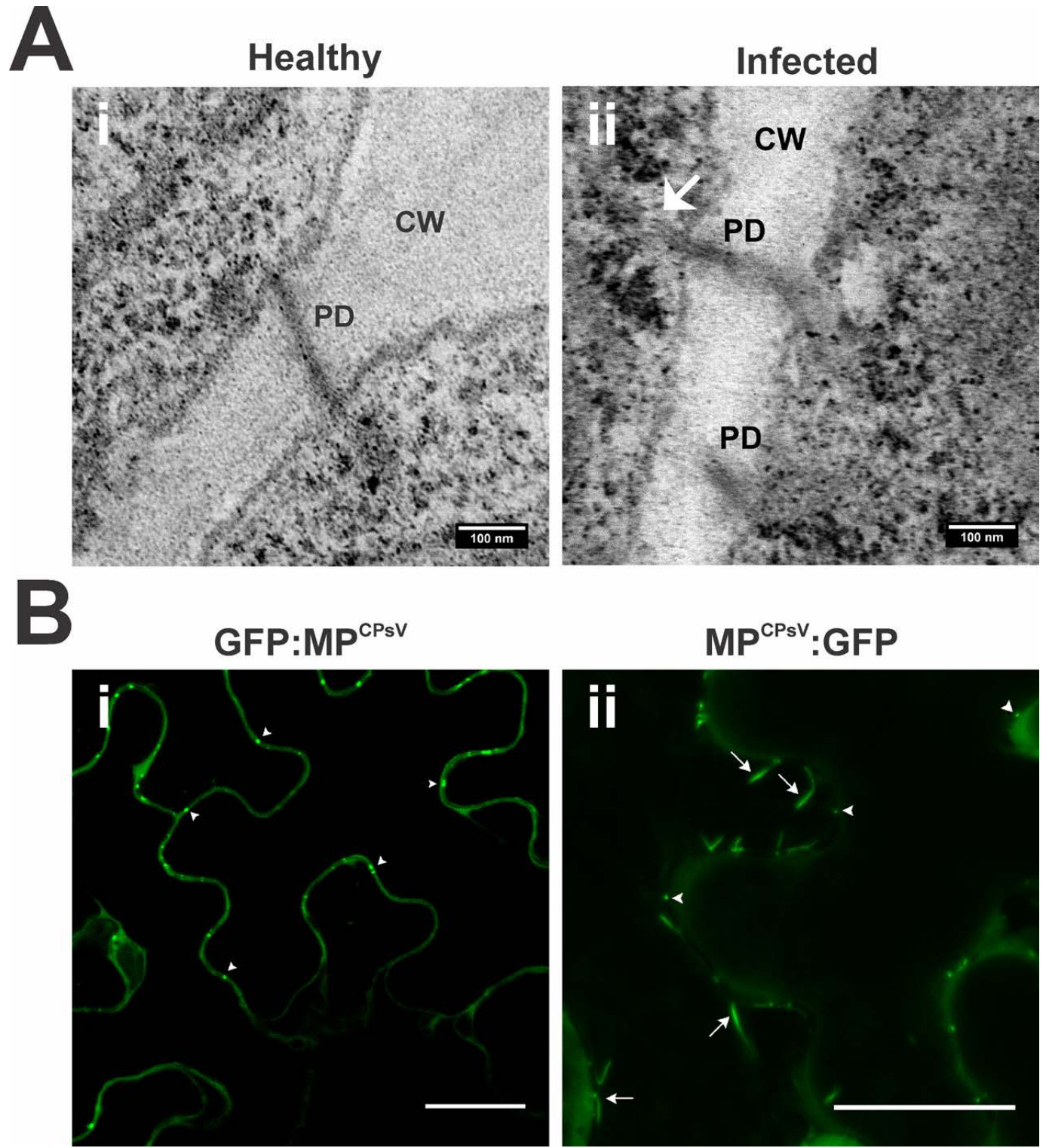
	MP ^{CPsV} :RFP + Sar1:GFP				MP ^{CPsV} :RFP + Sar1[H74L]:GFP			
	N° of fields with tubule-like structures at PD	N° of fields without tubule-like structures at PD	N° of fields observed	% of fields with tubule-like structures at PD	N° of fields with tubule-like structures at PD	N° of fields without tubule-like structures at PD	N° of fields observed	% of fields with tubule-like structures at PD
Assay 1	1	37	38	2,6	0	38	38	0
Assay 2	0	44	44	0	0	40	40	0
Assay 3	3	47	50	6	0	52	52	0
Total	4	128	132	3*	0	130	130	0

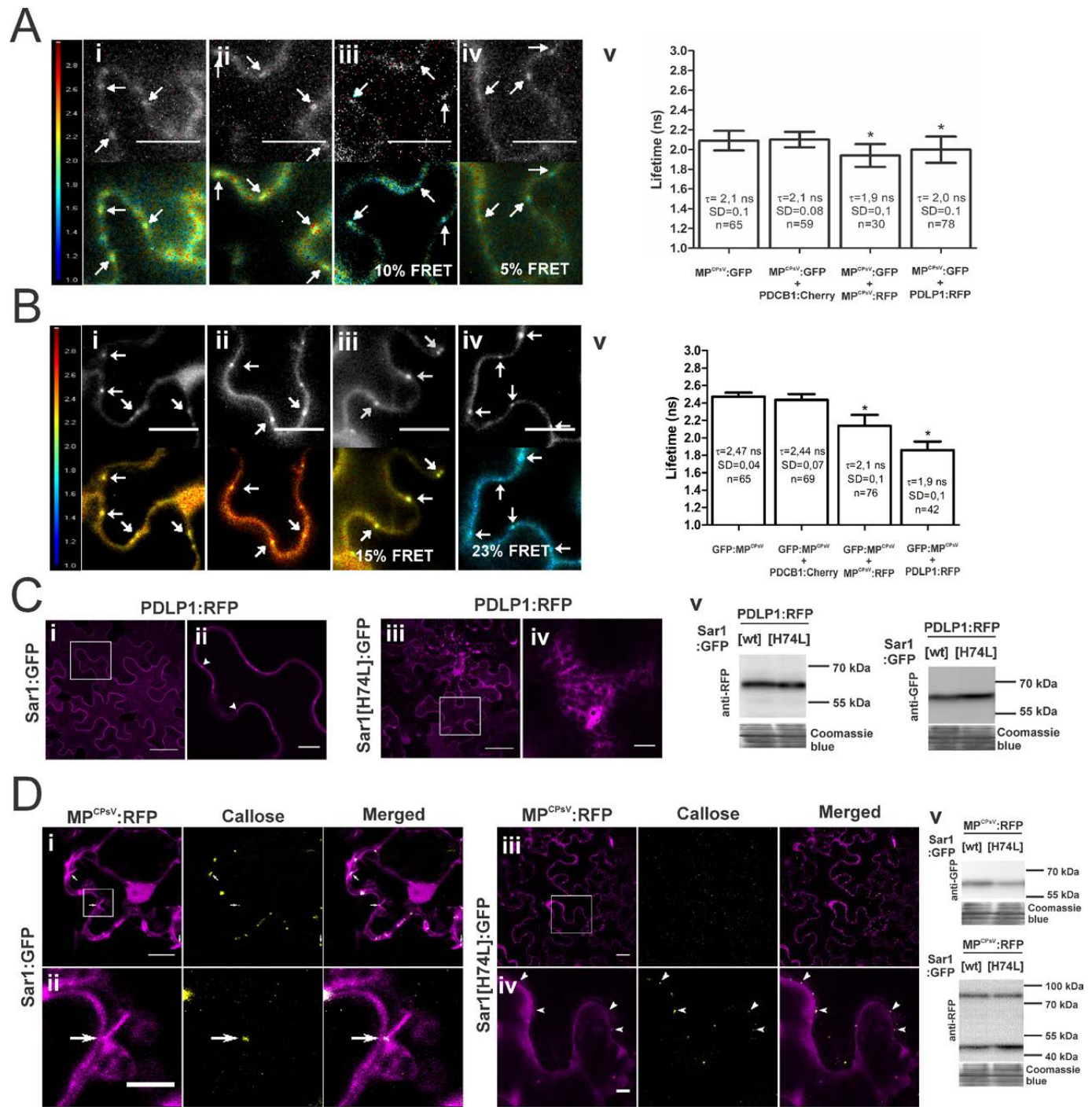
*represent statistical difference compared to Sar [H74L] unpaired t-test with p<0.01.

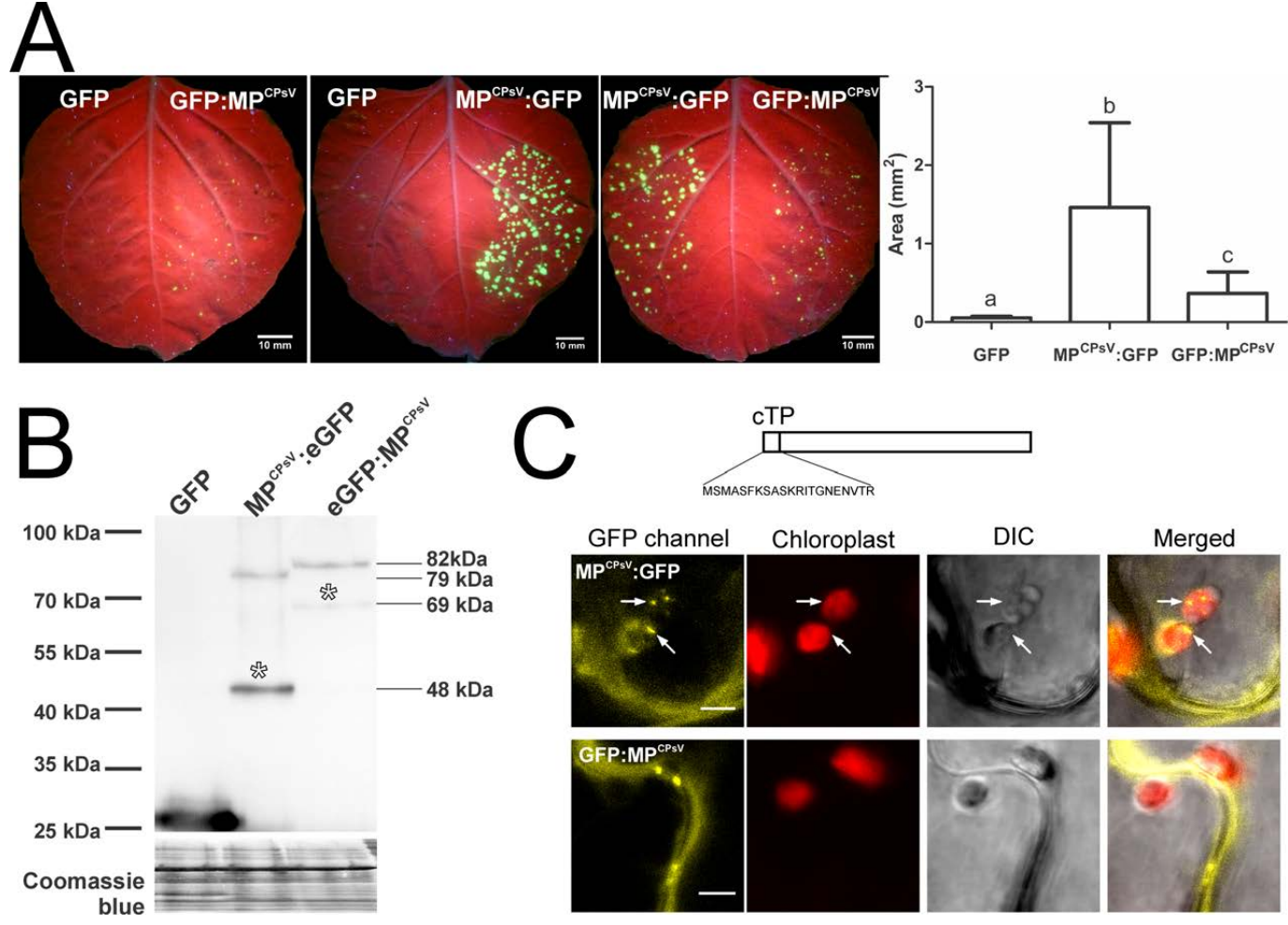
TABLE 2. 34K^{CPSV} tubule formation upon inhibition of the secretory pathway

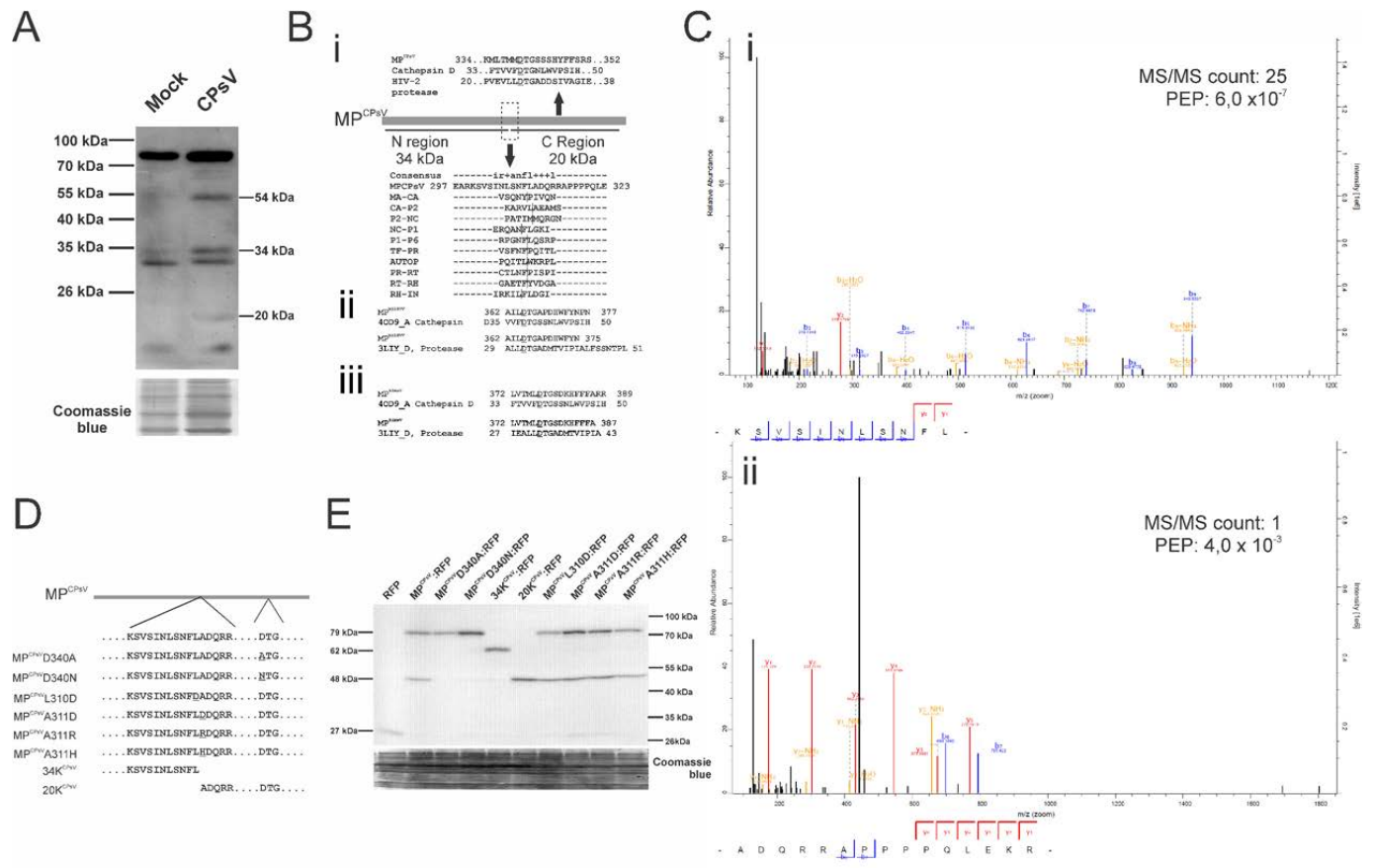
	34K ^{CPSV} :RFP + Sar1:GFP				34K ^{CPSV} :RFP + Sar1[H74L]:GFP			
	N° of fields with tubule-like structures at PD	N° of fields without tubule-like structures at PD	N° of fields observed	% of fields with tubule-like structures at PD	N° of fields with tubule-like structures at PD	N° of fields without tubule-like structures at PD	N° of fields observed	% of fields with tubule-like structures at PD
Assay 1	9	13	22	41	1	22	23	4
Assay 2	11	12	23	48	4	18	22	18
Assay 3	18	4	22	82	1	15	16	6
Total	38	29	67	57*	6	55	61	10

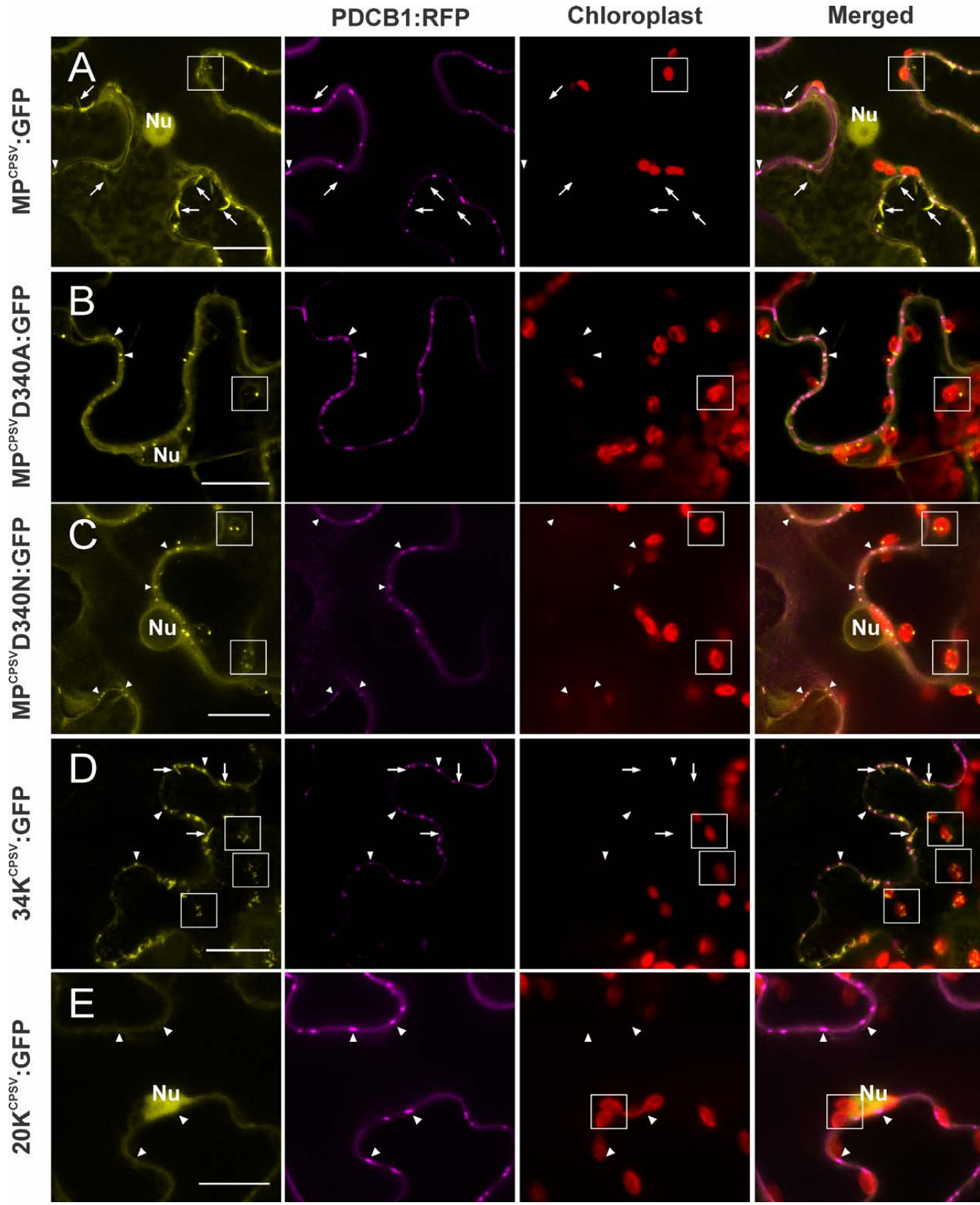
*represent statistical difference compared to Sar [H74L] unpaired t-test with p<0.05.

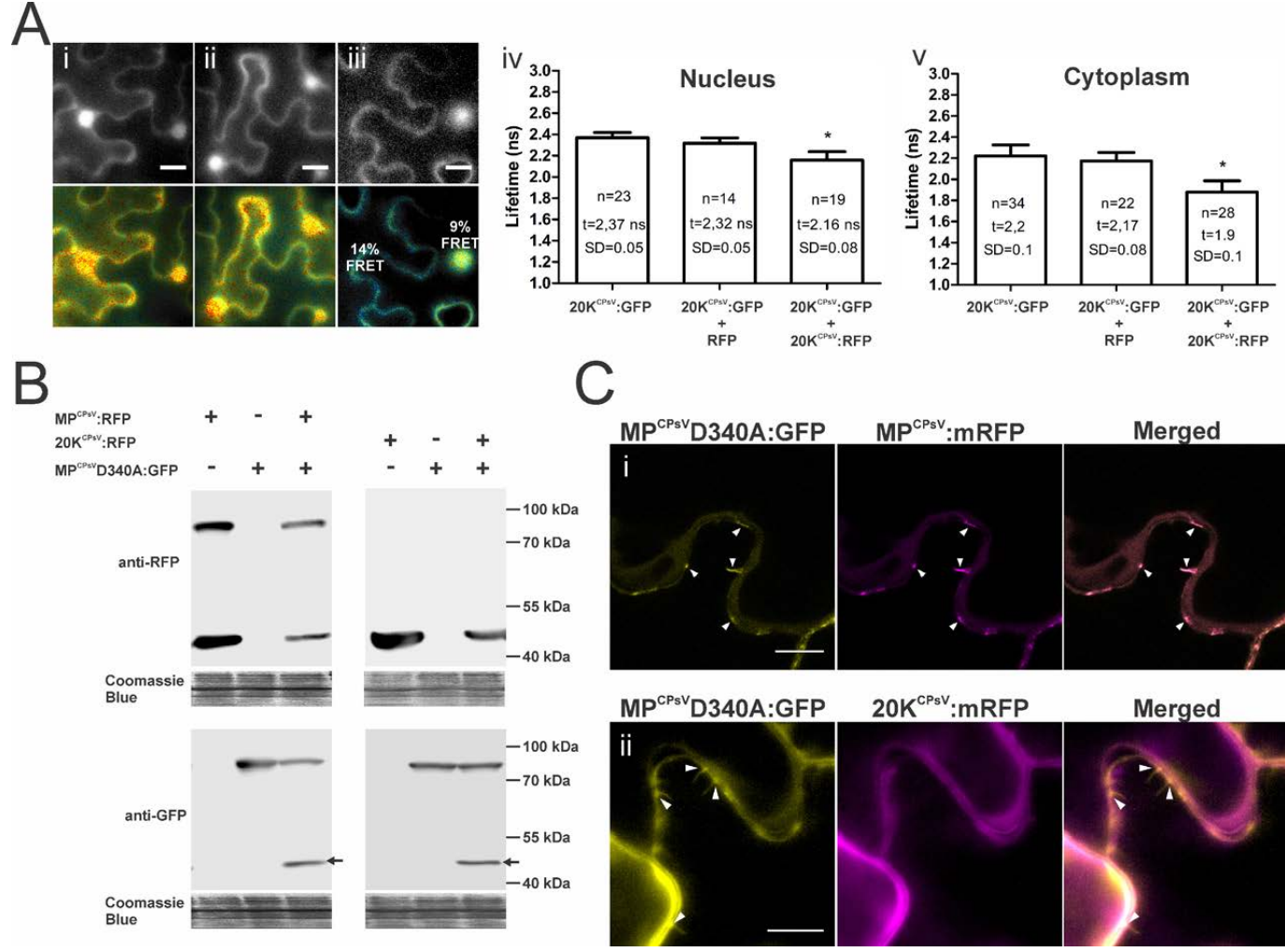




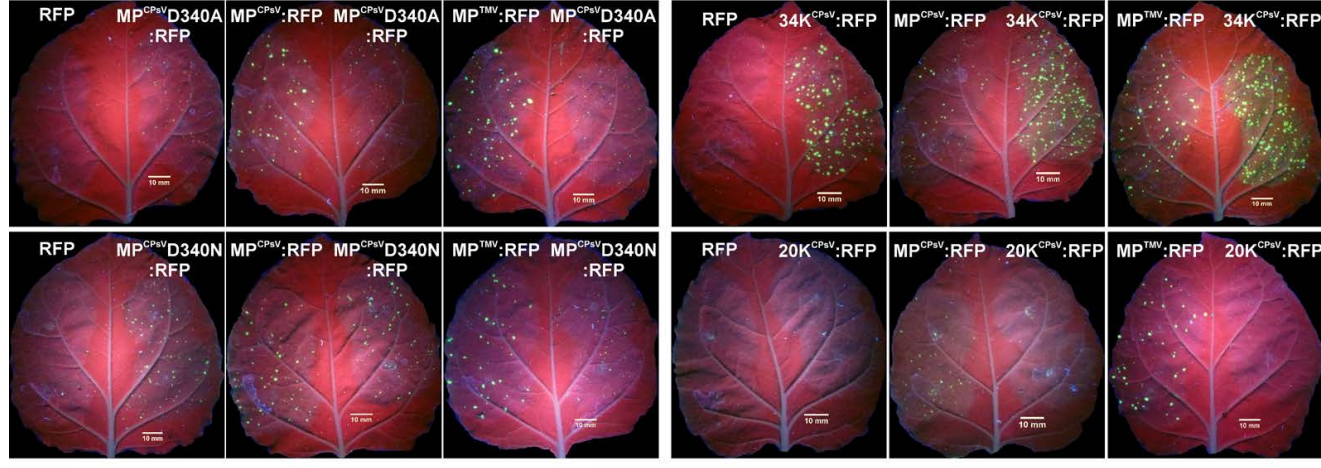




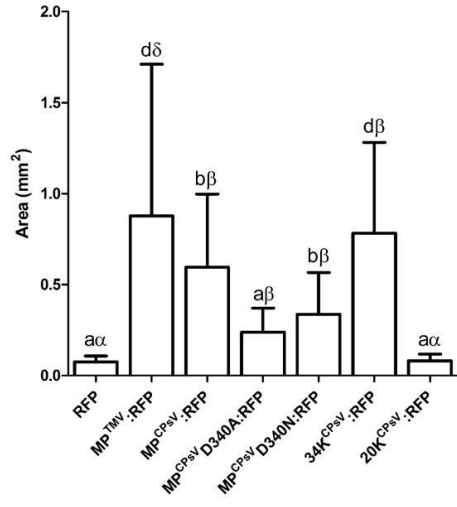




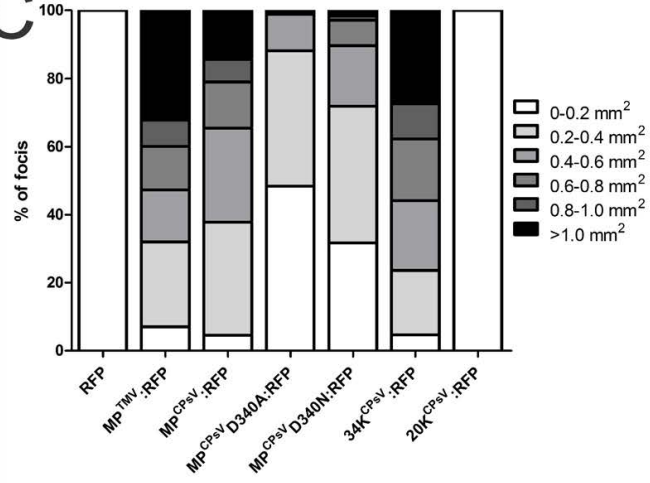
A



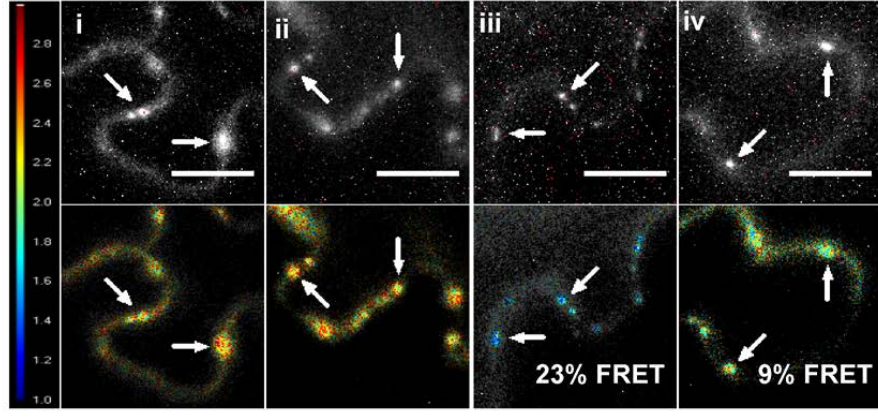
B



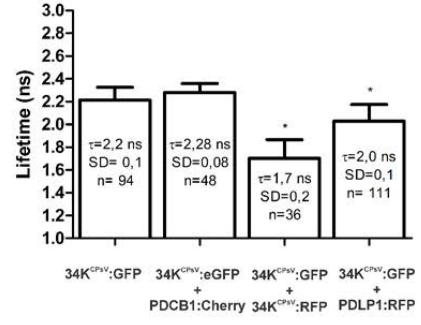
C



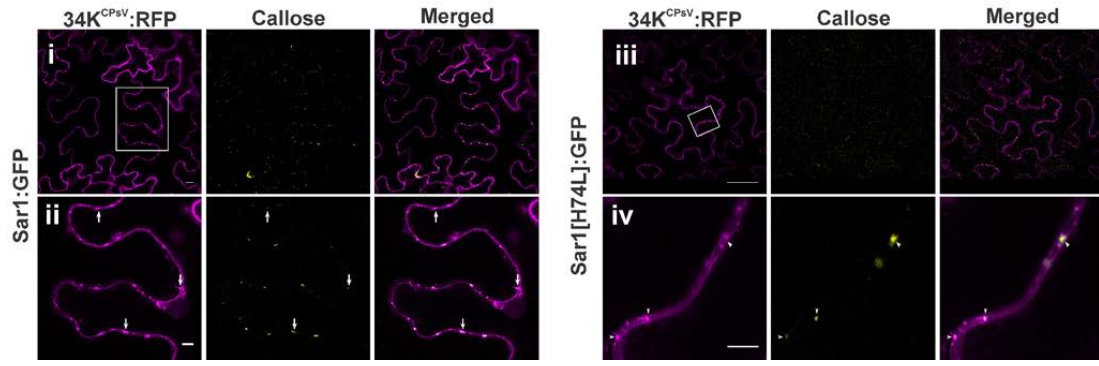
A



V



B



V

